GEOPHYSICS, VOL. 78, NO. 2 (MARCH-APRIL 2013); P. L1–L26, 18 FIGS., 1 TABLE.
10.1190/GEO2012-0160.1

On the propagation of a disturbance in a smoothly varying heterogeneous porous medium saturated with three fluid phases

D. W. Vasco[1]

ABSTRACT

From the equations governing the deformation of a porous medium containing three fluid phases, I derive expressions for the phase velocity of the various modes of displacement. These expressions are valid for a medium with smoothly varying heterogeneity. There is a single mode of transverse displacement, similar in nature to an elastic shear wave. The four-phase velocities of the longitudinal modes of displacement are derived from the solutions of a quartic equation. The coefficients of the polynomial equation are written as linear sums of the determinants of 4×4 matrices. The matrices contain various combinations of the parameters from the governing equations. The three-phase expressions are compared to two-phase estimates for the case in which one of the fluid saturations vanishes. Also, in a numerical illustration, velocity variations of around 10% are associated with the cyclic injection of carbon dioxide and water into an oil-saturated reservoir.

INTRODUCTION

In situations of practical interest, one must consider the flow of three fluids at depth. It is quite common for two immiscible liquid phases, such as oil and water, to be found within a reservoir, particularly after the onset of production. In addition, there can be an accompanying gas phase, such as air, steam, carbon dioxide, or methane, present within the reservoir pore volume. With advancements in recovery techniques and developments in environmental remediation, such instances of three-phase flow will become increasingly commonplace (Batzle et al., 1998). Three-phase flow can be quite complicated, particularly in the presence of such factors as gravitational effects due to density variation and lateral variations in properties such as permeability. Therefore, geophysical monitoring can be important in understanding three-phase flow within a reservoir (Hoversten et al., 2003). To this end, it is important to relate changes due to such flow to variations in seismic properties.

Currently, the most common approach for relating seismic properties to the presence of fluids is to combine Biot's theory for a porous rock saturated with a single fluid phase (Biot, 1956a, 1956b) with an approach for computing the composite bulk modulus of a fluid saturated rock (Gassmann, 1951; Smith et al., 2003). Multiple fluids are accommodated by computing effective fluid properties such as the density and bulk modulus, for a mixture (Batzle and Wang, 1992). In this way, any number of fluids might be accounted for. This approach has the advantage of simplicity and uses only essential parameters.

A more rigorous approach is to combine the properties of the individual constituents, along with the flow properties of the porous rock, including such features as absolute permeability, relative permeability properties, and capillary pressure properties. Such approaches are too numerous to provide a comprehensive review in this Introduction. Therefore, I point out some representative studies that treated single phase flow (Garg, 1971; Pride et al., 1992), and two-phase flow (Berryman et al., 1988; Santos, 1990; Tuncay, 1995; Tuncay and Corapcioglu, 1996, 1997; Lo et al., 2005, 2009) for a homogeneous medium. Recently, the two-phase work was extended to a medium containing smoothly varying heterogeneity in Vasco and Minkoff (2012). These papers dealt with large-scale, wave-induced flow, the so-called macroscopic flow. It has been pointed out that there are other scales of flow that may be important with regard to seismic wave propagation through a porous medium. There is a small-scale (microscopic) fluid migration from microcracks, including grain contacts, referred to as squirt-flow (Biot, 1962b; Mavko and Nur, 1975; O'Connell and Budianski, 1977; Jones, 1986; Dvorkin et al., 1994). This effect has been incorporated into the Biot model (Pham et al., 2002). Also, an intermediate or mesoscopic flow, due to wave-induced flow on a scale smaller

Manuscript received by the Editor 1 May 2012; revised manuscript received 24 October 2012; published online 5 March 2013.
[1]Berkeley Laboratory, Earth Sciences Division, Berkeley, California, USA. E-mail: dwvasco@lbl.gov.

than the wavelength of the elastic wave but larger than the pore scale was first proposed by White (1975) and explored in more depth by Pride et al. (2004). The microscopic and the mesoscopic flow have been adopted into a single phase Biot type model (JafarGandomi and Curtis, 2011).

In this paper, I extend the two-phase work of Vasco and Minkoff (2012) to the case in which there are three fluid phases. Specifically, I consider the zeroth-order terms of an asymptotic analysis of the equations governing the coupled deformation and flow in a heterogeneous porous medium containing three fluids. The resulting linear system of equations is used to derive expressions for the slowness and hence the phase velocity of the various modes of displacement. For the purposes of this paper, I use Biot's (1956a, 1956b) theory of macroscopic flow to relate the coefficients of the poroelastic governing equations to the rock, fluid, and flow properties, as detailed in Appendix A, but the other methods just noted can be used to account for microscopic and mesoscopic flow.

METHODOLOGY

The governing equations

I consider a porous medium saturated with three immiscible fluid phases That is, if S_i denotes the saturation of the ith phase, then in the available pore space

$$\sum_{i=1}^{3} S_i = S_1 + S_2 + S_3 = 1. \tag{1}$$

For a given unit volume of fluid-filled porous rock, with porosity ϕ, I denote the fraction of the ith fluid as

$$\alpha_i = \phi S_i. \tag{2}$$

The three phases are assumed to behave as Newtonian fluids, representing liquids and/or gases moving through the pore space of the solid matrix. The components of the solid are assumed to react elastically. Thus, the composite body acts as a poroelastic material.

As shown in Tuncay and Corapcioglu (1996), under the assumptions of negligible mass exchange between the phases, small deformation, a seismic wavelength much larger then the microscopic scale, and a linearization of the density variation, the average momentum equations reduce to

$$\alpha_s \rho_s \frac{\partial \dot{\mathbf{u}}_s}{\partial t} = \alpha_s \nabla \cdot \sigma_s - \sum_{j=1}^{3} \mathbf{d}_j \tag{3}$$

and

$$\alpha_i \rho_i \frac{\partial \dot{\mathbf{u}}_i}{\partial t} = \alpha_i \nabla \cdot \sigma_i + \mathbf{d}_i, \tag{4}$$

where the solid and fluid displacements are denoted by $\mathbf{u}_s$ and $\mathbf{u}_i$, ρ_s is the density of the solid components while ρ_i is the density of the ith fluid, σ_s and σ_i are the respective stress tensors, and the dots over the displacement vectors denote time derivatives. In an effort to keep the presentation compact, I represent the three equations for the fluid phases by a single indexed equation 4, allowing i to take the values 1, 2, and 3 for the respective fluid phases. The vectors $\mathbf{d}_i$ are the momentum transfer vectors or interaction terms, representing drag forces due to the interaction of the fluids with the solid matrix (Pride et al., 1993). Pride et al. (1992) argue that the drag forces can be written in the specific form

$$\mathbf{d}_i = \rho_i \alpha_i \nu (1+\nu)^{-1} \frac{\partial \dot{\mathbf{w}}_i}{\partial t}, \tag{5}$$

where $\dot{\mathbf{w}}_i$ is the flow velocity of fluid i. The flow velocity of the fluid phase is measured relative to the current position of the solid, given by $\dot{\mathbf{w}}_i = \dot{\mathbf{u}}_i - \dot{\mathbf{u}}_s$. The quantity $(1+\nu)^{-1}$ is referred to as the "dynamic tortuosity" by Johnson et al. (1987). The dynamic tortuosity controls how much fluid flows in response to the applied forces. The variable ν may be thought of as a convolutional operator in the time domain, or as a frequency-dependent coefficient in the frequency domain, related to the interaction of the fluid and the solid (Pride et al., 1992, 1993).

If I substitute the expression 5 for $\mathbf{d}_i$, define the coefficient

$$D_i = \rho_i \alpha_i \nu (1+\nu)^{-1}, \tag{6}$$

and add and subtract $\alpha_i \rho_i \partial \dot{\mathbf{u}}_s / \partial t$ from the left side of equation 4, then I can write equations 3 and 4 as

$$\alpha_s \rho_s \frac{\partial \dot{\mathbf{u}}_s}{\partial t} + \sum_{j=1}^{3} D_j \frac{\partial \dot{\mathbf{w}}_j}{\partial t} = \alpha_s \nabla \cdot \sigma_s \tag{7}$$

$$\alpha_i \rho_i \frac{\partial \dot{\mathbf{u}}_i}{\partial t} + (\alpha_i \rho_i - D_i) \frac{\partial \dot{\mathbf{w}}_i}{\partial t} = \alpha_i \nabla \cdot \sigma_i. \tag{8}$$

Taking the Fourier transform of equations 7 and 8, defining

$$\nu_s = \alpha_s \rho_s \omega^2, \tag{9}$$

$$\nu_i = \alpha_i \rho_i \omega^2, \tag{10}$$

$$\xi_i = \alpha_i \rho_i \nu (1+\nu)^{-1} \omega^2, \tag{11}$$

and

$$\Gamma_i = \alpha_i \rho_i [1 - \nu (1+\nu)^{-1}] \omega^2, \tag{12}$$

I can write equations 7 and 8 in the frequency domain

$$\alpha_s \nabla \cdot \sigma_s + \nu_s \mathbf{U}_s + \sum_{j=1}^{3} \xi_j \mathbf{W}_j = 0 \tag{13}$$

$$\alpha_i \nabla \cdot \sigma_i + \nu_i \mathbf{U}_s + \Gamma_i \mathbf{W}_i = 0, \tag{14}$$

where the capital letters signify the Fourier transform of the respective time-domain quantities.

To complete the formulation, I need to write equations 13 and 14 solely in terms of the solid and fluid displacements, $\mathbf{U}_s$ and $\mathbf{W}_i, i = 1, 2, 3$. Assuming a linear poroelastic constitutive relationship relating the stress tensors to the displacements, I can write 13 and 14 as

$$\nabla \cdot G_m \left[\nabla \mathbf{U}_s + \nabla(\mathbf{U}_s)^T - \frac{2}{3}\nabla \cdot \mathbf{U}_s \mathbf{I}\right] + \nabla\left[K_u \nabla \cdot \mathbf{U}_s + \sum_{j=1}^{3} C_{sj} \nabla \cdot \mathbf{W}_j\right] + \nu_s \mathbf{U}_s + \sum_{j=1}^{3} \xi_j \mathbf{W}_j = 0 \quad (15)$$

$$\nabla[C_{is} \nabla \cdot \mathbf{U}_s + \Sigma_{j=1}^{3} M_{ij} \nabla \cdot \mathbf{W}_j] + \nu_i \mathbf{U}_s + \Gamma_i \mathbf{W}_i = 0. \quad (16)$$

The coefficients of the effective poroelastic medium depend upon the properties of the fluids contained within the pores and on the nature of the rock and its constituents. There are now numerous constitutive models relating the properties of the components of a porous medium to the effective elastic coefficients. The early model of Biot (1962a) for a single fluid has been particularly influential and has been extended to a medium containing two fluid phases (Berryman et al., 1988; Santos et al., 1990; Tuncay and Corapcioglu, 1996; Lo et al., 2005).

In Appendix A, I extend the approach of Tuncay and Corapcioglu (1996) to a porous medium containing three fluid phases. There, the coefficients are defined in terms of the properties of the fluids, the properties of the solid constituents, and the properties of the porous rock, including the capillary pressure functions. Note that it is possible to further generalize the coefficients by adopting the theories listed in the Introduction to this paper. That is, I could account for fluid flow into microcracks (Biot, 1962b; Dvorkin et al., 1994) and mesoscopic flow (White, 1975; Pride et al., 2004) perhaps in the fashion described in Carcione and Gurevich (2011). Regardless of the theory used to set up the equations of poroelasticity, and hence the complex, frequency-dependence of the coefficients, the techniques described in the remainder of this paper are still applicable and the expressions for the slownesses in a heterogeneous medium are still valid.

I wish to point out that, although there are a large number of derived parameters in the constitutive relationship outlined in Appendix A, there are only a handful of fundamental quantities underlying all of the derived parameters. The 12 basic parameters are listed in Table 1. The two right-most columns signify two sets of values used in the Applications section. The first set involved homogeneous distributions of two and three fluids within a homogeneous porous rock. The second set is associated with the simulation of an enhanced oil recovery (EOR) operation in which carbon dioxide gas and water are injected in a cyclic fashion into an oil bearing reservoir. In that case, many of the properties vary spatially within the reservoir and hence are labeled as "variable". Note that for some, such as the densities and compressibilities, there are values for each fluid phase and for the solid phase. There are three major categories into which the parameters may be classified. However, there is overlap between the various categories and they are not exclusive. The attributes of the solid: the bulk modulus of the solid grains or particles, K_s, the density of the solid, ρ_s, and the frame moduli of the porous matrix, K_{fr} (bulk) and G_{fr} (shear) are listed first in Table 1. Second, there are the properties associated with the three fluid phases: the bulk moduli of the fluids (K_i), the densities of the fluid components (ρ_i), and the viscosities of the fluid phases (μ_i). Finally, there are the flow properties of the poroelastic medium, that is the porosity (ϕ), the absolute permeability (k), the relative permeabilities (k_{ri}), and the capillary pressure properties (P_{c12} and P_{c13}). The

Table 1. Table listing the 12 fundamental parameters required to compute the transverse and longitudinal phase velocities and attenuations at a particular frequency.

Category	Parameter	Description (units)	Multiphase applications	CO_2 simulation
Solid	K_s	Grain bulk modulus (Pa)	35.00×10^9	34.00×10^9
	ρ_s	Grain density (kg/m^3)	2650.00	2650.00
	K_{fr}	Frame bulk modulus (Pa)	8.33×10^6	1.50×10^9
	G_{fr}	Frame shear modulus (Pa)	3.85×10^6	1.00×10^9
Fluids	K_j	Bulk modulus (Pa)	2.25×10^9 (Water) 0.14×10^6 (Air) 0.57×10^9 (Oil)	Variable
	ρ_j	Density (kg/m^3)	997.00 (Water) 1.10 (Air) 762.00 (Oil)	Variable
	μ_j	Viscosity (Pa-s)	1.00×10^{-3} (Water) 18.00×10^{-6} (Air) 1.44×10^{-3} (Oil)	Variable
	S_j	Saturation (fraction)	Variable	Variable
Flow	k	Static permeability (m^2)	8.00×10^{-13}	0.50×10^{-13}
	ϕ	Porosity (fraction)	0.45	0.30
	k_{rj}	Relative permeability (m^2)	Variable	Variable
	P_{cij}	Capillary pressure (Pa)	Variable	Variable

first two, ϕ and k, could easily been included as properties of the solid. I list them as flow properties because they are of primary importance in the modeling of fluid flow in the subsurface. In fact, absolute permeability, k, is a quantity of great interest due to its role in controlling fluid flow. All of these parameters are contained in the coefficients in equations 9, 10, 11, and 12 and in the matrix $\mathbf{K}$ given by the expression A-25. Some of the flow properties enter through the variable ν, a quantity related to the dynamic tortuosity, as shown in the Applications section (see equations 55 and 56). Note that there is also the frequency, a general parameter that influences aspects of the propagation such as the velocity and the attenuation. I do not include it in Table 1 because it is an independent parameter and is not a property of either the solid or the fluid.

Asymptotic analysis

The governing equations 15 and 16 are rather formidable, relating four coupled vectors, with coefficients that depend upon spatial position and with some coefficients that are functions of frequency. To work toward a solution and to gain insight, some simplification is required. For this purpose, I adopt an asymptotic approach, motivated by the idealization of a smoothly varying heterogeneous medium. That is, I shall assume that, away from boundaries such as layering and faults, the length scale of the heterogeneity is much larger than the length scale of any propagating disturbance. Such an assumption is compatible with the goal of using seismic observations to characterize variations in reservoir properties, that is, solving the inverse problem. In inverse problems, one can typically only recover large-scale variations in reservoir properties due to limited resolution (Menke, 1989). Thus, the models of interest will consist of smoothly varying perturbations added to the original background model.

To specify the asymptotic expansion, consider a parameter D representing the length scale of the heterogeneity. Furthermore, let d represent the length scale associated with a propagating disturbance, for example the spatial wavelength of a pulse. Define a scale parameter ε as the ratio of the length scales

$$\varepsilon = \frac{d}{D}, \tag{17}$$

and because $d \ll D$ one also has $\varepsilon \ll 1$. I frame the problem in terms of slow coordinates $\mathbf{X}$, the spatial coordinates $\mathbf{x}$ scaled by ε

$$\mathbf{X} = \varepsilon \mathbf{x}, \tag{18}$$

creating an implicit dependence of the solution vectors $\mathbf{U}_s$ and $\mathbf{W}_i$ upon ε.

Asymptotic expressions for the displacements

The asymptotic expansion is a series representation of the displacement vectors in terms of powers of the scale parameter ε

$$\mathbf{U}_s(\mathbf{X}, \omega, \theta) = e^{i\theta} \sum_{n=0}^{\infty} \varepsilon^n \mathbf{U}_s^n(\mathbf{X}, \omega) \tag{19}$$

$$\mathbf{W}_i(\mathbf{X}, \omega, \theta) = e^{i\theta} \sum_{n=0}^{\infty} \varepsilon^n \mathbf{W}_i^n(\mathbf{X}, \omega), \tag{20}$$

where $\theta(\mathbf{x}, \omega)$ is a function, referred to as the "local phase," related to the kinematics, or the traveltime, of the propagating disturbance (Whitham, 1974; Anile et al., 1993). The functions $\mathbf{U}_s^n(\mathbf{X}, \omega)$ and $\mathbf{W}_i^n(\mathbf{X}, \omega)$ represent the amplitudes of the displacements and their successive corrections. The series 19 and 20 are generalized plane-wave expansions of the solid and fluid displacement fields in the frequency domain (Friedlander and Keller, 1955; Luneburg, 1966; Kline and Kay, 1965; Chapman, 2004). Because the expansion parameter ε is assumed to be small, the heterogeneity is assumed to vary smoothly, only the first few terms of the series are significant. For example, the zeroth-order term is often used to represent the solution (Kline and Kay, 1965; Vasco et al., 2003).

To completely transform the governing equations 15 and 16, I rewrite the derivative operators in terms of the slow coordinates. For example, the partial derivative of $\mathbf{U}_s$ with respect to the spatial coordinate x_i becomes

$$\frac{\partial \mathbf{U}_s}{\partial x_i} = \frac{\partial X_i}{\partial x_i}\frac{\partial \mathbf{U}_s}{\partial X_i} + \frac{\partial \theta}{\partial x_i}\frac{\partial \mathbf{U}_s}{\partial \theta}, \tag{21}$$

and hence, making use of equation 18,

$$\frac{\partial \mathbf{U}_s}{\partial x_i} = \varepsilon \frac{\partial \mathbf{U}_s}{\partial X_i} + \frac{\partial \theta}{\partial x_i}\frac{\partial \mathbf{U}}{\partial \theta} \tag{22}$$

(Anile et al., 1993). Thus, the differential operators are likewise written as

$$\nabla \mathbf{U}_s = \varepsilon \nabla_{\mathbf{X}} \mathbf{U}_s + \nabla\theta \frac{\partial \mathbf{U}_s}{\partial \theta}, \tag{23}$$

where $\nabla_{\mathbf{X}}$ denotes the gradient with respect to the components of the slow variables $\mathbf{X}$. In what follows, I shall drop the subscript $\mathbf{X}$ from the gradient operator in slow coordinates.

Terms of zeroth-order: The phase of the disturbance

Asymptotic solutions are obtained by rewriting the governing equations in slow coordinates and transforming derivative operators as in expression 22. Next, the power series expansions 19 and 20 are inserted into the transformed governing equations. The result is a set of four vector equations, each containing terms of various orders in ε. Because $\varepsilon \ll 1$, only the lowest-order terms are retained. This procedure was presented in detail in Vasco (2009) and Vasco and Minkoff (2012) for propagation in a porous medium containing one and two fluid phases, respectively. Because the approach has been described in detail in these two studies, I shall only present the results of the asymptotic analysis. Specifically, the terms of zeroth-order in ε are contained in the following equations

$$\alpha \mathbf{U}_s^0 - \beta \mathbf{l} \cdot \mathbf{U}_s^0 \mathbf{l} + \sum_{j=1}^{3} (\xi_j \mathbf{W}_j^0 - C_{sj} \mathbf{l} \cdot \mathbf{W}_j^0 \mathbf{l}) = 0 \tag{24}$$

$$\nu_i \mathbf{U}_s^0 - C_{is} \mathbf{l} \cdot \mathbf{U}_s^0 \mathbf{l} + \Gamma_i \mathbf{W}_i^0 - \sum_{j=1}^{3} M_{ij} \mathbf{l} \cdot \mathbf{W}_j^0 \mathbf{l} = 0, \tag{25}$$

where $\mathbf{U}_s^0$ and $\mathbf{W}_i^0$ are the zeroth-order amplitude functions in equations 19 and 20,

$$\mathbf{l} = \nabla\theta \tag{26}$$

is the phase gradient vector,

$$\alpha = \nu_s - G_m l^2 \tag{27}$$

and

$$\beta = K_u + \frac{1}{3}G_m, \tag{28}$$

where $l = |\nabla\theta|$ is magnitude of the vector $\mathbf{l}$. The set of equations 24 and 25 may be written as the matrix equation

$$(\mathbf{A} - \mathbf{B})\mathbf{U} = \mathbf{0}, \tag{29}$$

where

$$\mathbf{A} = \begin{pmatrix} \alpha\mathbf{I} & \xi_1\mathbf{I} & \xi_2\mathbf{I} & \xi_3\mathbf{I} \\ \nu_1\mathbf{I} & \Gamma_1\mathbf{I} & \mathbf{0} & \mathbf{0} \\ \nu_2\mathbf{I} & \mathbf{0} & \Gamma_2\mathbf{I} & \mathbf{0} \\ \nu_3\mathbf{I} & \mathbf{0} & \mathbf{0} & \Gamma_3\mathbf{I} \end{pmatrix}, \tag{30}$$

$$\mathbf{B} = \begin{pmatrix} \beta\mathbf{l}\mathbf{l}^T & C_{s1}\mathbf{l}\mathbf{l}^T & C_{s2}\mathbf{l}\mathbf{l}^T & C_{s3}\mathbf{l}\mathbf{l}^T \\ C_{1s}\mathbf{l}\mathbf{l}^T & M_{11}\mathbf{l}\mathbf{l}^T & M_{12}\mathbf{l}\mathbf{l}^T & M_{13}\mathbf{l}\mathbf{l}^T \\ C_{2s}\mathbf{l}\mathbf{l}^T & M_{21}\mathbf{l}\mathbf{l}^T & M_{22}\mathbf{l}\mathbf{l}^T & M_{23}\mathbf{l}\mathbf{l}^T \\ C_{3s}\mathbf{l}\mathbf{l}^T & M_{31}\mathbf{l}\mathbf{l}^T & M_{32}\mathbf{l}\mathbf{l}^T & M_{33}\mathbf{l}\mathbf{l}^T \end{pmatrix}, \tag{31}$$

and

$$\mathbf{U} = \begin{pmatrix} \mathbf{U}_s^0 \\ \mathbf{W}_1^0 \\ \mathbf{W}_2^0 \\ \mathbf{W}_3^0 \end{pmatrix}. \tag{32}$$

The quantity $\mathbf{I}$ in the matrix $\mathbf{A}$ is the 3×3 identity matrix with ones on the diagonal and zeros off of the diagonal. The quantity $\mathbf{l}\mathbf{l}^T$ is the outer product of the column vector $\mathbf{l}$, which may be thought of as a 3×1 matrix, and the row vector $\mathbf{l}^T$, which may be thought of as a 1×3 matrix. One may also think of $\mathbf{l}\mathbf{l}^T$ as a dyadic, a generalization of a vector to a matrix (Spiegel, 1959, p. 73; Ben-Menahem and Singh, 1981).

The system of equations 29 has a nontrivial solution $\mathbf{U}$ if the determinant of the coefficient matrix vanishes (Noble and Daniel, 1977, p. 203)

$$\det\,(\mathbf{A} - \mathbf{B}) = 0. \tag{33}$$

Because the elements of the matrices $\mathbf{A}$ and $\mathbf{B}$ contain the coefficients in the governing equations, and the components of $\mathbf{l} = \nabla\theta$, equation 33 is a differential equation for θ. This differential equation, with coefficients that depend upon spatial coordinates and the frequency, ω, is the eikonal equation determining the propagation time of a disturbance through a heterogeneous medium saturated with three fluid phases. Because the coefficients may depend upon frequency, the propagation is likely to be dispersive.

The matrices $\mathbf{A}$ and $\mathbf{B}$ are 12×12 and the determinant in equation 33 is a 12th-order polynomial in the elements of the matrices. Furthermore, the elements of these matrices contain product terms of the vector components of $\mathbf{l}$. For example, the matrix $\mathbf{B}$ contains product terms of the form $\mathbf{l}\mathbf{l}^T$. Thus, the polynomial equation is of degree 24 in the components of $\mathbf{l}$. A direct formulation of the polynomial determined by equation 33 will lead to some rather involved algebra.

Rather than computing the determinant directly, I take an alternative approach and work with the eigenvalues and eigenvectors of the matrix $(\mathbf{A} - \mathbf{B})$. This approach makes use of the fact that the determinant of a matrix is the product of the eigenvalues of the matrix (Noble and Daniel, 1977, p. 264). Thus, the determinant of the matrix vanishes when one or more of the eigenvalues vanishes. If I denote the eigenvalue by λ, and the corresponding eigenvector by $\mathbf{e}$ then I have that

$$(\mathbf{A} - \mathbf{B})\mathbf{e} = \lambda\mathbf{I}\mathbf{e} = \mathbf{0}. \tag{34}$$

For a nontrivial eigenvector $\mathbf{e}$, condition 34 is equivalent to equation 33, so one gains no mathematical advantage from reformulating the problem. However, motivated by the structure of the matrices $\mathbf{A}$ and $\mathbf{B}$ and some insight from the nature of wave propagation, I can specify the form of the eigenvectors $\mathbf{e}$ and simplify equation 34.

With regard to the structure of the matrices $\mathbf{A}$ and $\mathbf{B}$, given by 30 and 31, there is a certain homogeneity in the coefficients of each matrix. In particular, the matrix $\mathbf{A}$ has a block matrix structure and may be thought of as a 4×4 matrix with elements that contain the identity matrix (the zero elements may be thought of as $0 \times \mathbf{I}$). Similarly, the matrix $\mathbf{B}$ is a 4×4 block matrix with all blocks containing the matrix $\mathbf{l}\mathbf{l}^T$. The vector direction $\mathbf{l}$ has special significance because when multiplied by $\mathbf{A}$ or $\mathbf{B}$ the block elements return either the vector $\mathbf{l}$ or the zero vector. Similarly, the two vector directions perpendicular to $\mathbf{l}$ which we denote by $\mathbf{l}_1^\perp$ and $\mathbf{l}_2^\perp$, return their values or zero when multiplied by $\mathbf{A}$ and zero when multiplied by $\mathbf{B}$. Thus, vectors of the form

$$\mathbf{e}^l = \begin{pmatrix} l_s\mathbf{l} \\ l_1\mathbf{l} \\ l_2\mathbf{l} \\ l_3\mathbf{l} \end{pmatrix}, \tag{35}$$

$$\mathbf{e}_1^\perp = \begin{pmatrix} t_s\mathbf{l}_1^\perp \\ t_1\mathbf{l}_1^\perp \\ t_2\mathbf{l}_1^\perp \\ t_3\mathbf{l}_1^\perp \end{pmatrix}, \tag{36}$$

and

$$\mathbf{e}_2^\perp = \begin{pmatrix} s_s\mathbf{l}_2^\perp \\ s_1\mathbf{l}_2^\perp \\ s_2\mathbf{l}_2^\perp \\ s_3\mathbf{l}_2^\perp \end{pmatrix}, \tag{37}$$

return either scaled versions of themselves or zero when multiplied by the elements of the matrices of $\mathbf{A}$ and $\mathbf{B}$. This suggests that, when I substitute each of these vectors into equation 34, the result will be four equations in the four unknown coefficients of each vector.

The forms of the vectors $\mathbf{e}^l$, $\mathbf{e}_1^\perp$, and $\mathbf{e}_2^\perp$ also have physical significance and represent well-known modes of wave propagation. For example, the vector $\mathbf{e}^l$ represents longitudinal wave propagation, in which the solid and fluid displacements are parallel to the direction of propagation $\mathbf{l} = \nabla\theta$ (Chapman, 2004). Conversely, the vectors $\mathbf{l}_1^\perp$ and $\mathbf{l}_2^\perp$ signify transverse displacements, displacements perpendicular to the direction of propagation, similar to an elastic shear wave. Longitudinal and transverse modes are solutions of the elastic wave equation in a homogeneous medium (Aki and Richards, 1980, p. 68; Chapman, 2004, p. 111) as well as high-frequency solutions for a heterogeneous isotropic medium (Aki and Richards, 1980, p. 89). Longitudinal and transverse modes are also documented for waves in homogeneous poroelastic media containing a single fluid (Pride, 2005) and two fluids (Tuncay and Corapcioglu, 1996). The three vectors $\mathbf{e}^l$, $\mathbf{e}_1^\perp$, and $\mathbf{e}_2^\perp$ are linearly independent and may be used to represent all modes of propagation. In the subsections that follow, I shall consider the transverse and longitudinal modes of propagation in succession.

The transverse mode of propagation

Because the transverse mode of propagation is somewhat simpler due to the vanishing of all contributions from the matrix $\mathbf{B}$, I begin by considering the vector $\mathbf{e}_1^\perp$. The treatment of the other transverse eigenvector $\mathbf{e}_2^\perp$ is similar and will produce an identical slowness, or corresponding velocity. The eigenvector equation 34 reduces to

$$\begin{pmatrix} \alpha\mathbf{I} & \xi_1\mathbf{I} & \xi_2\mathbf{I} & \xi_3\mathbf{I} \\ \nu_1\mathbf{I} & \Gamma_1\mathbf{I} & \mathbf{0} & \mathbf{0} \\ \nu_2\mathbf{I} & \mathbf{0} & \Gamma_2\mathbf{I} & \mathbf{0} \\ \nu_3\mathbf{I} & \mathbf{0} & \mathbf{0} & \Gamma_3\mathbf{I} \end{pmatrix} \begin{pmatrix} t_s\mathbf{l}_1^\perp \\ t_1\mathbf{l}_1^\perp \\ t_2\mathbf{l}_1^\perp \\ t_3\mathbf{l}_1^\perp \end{pmatrix} = \begin{pmatrix} \mathbf{0} \\ \mathbf{0} \\ \mathbf{0} \\ \mathbf{0} \end{pmatrix}. \tag{38}$$

This equation has a nontrivial solution if the determinant of the coefficient matrix vanishes. Due to the structure of the matrix $\mathbf{A}$ and of the vector $\mathbf{e}_1^\perp$, this condition is equivalent to

$$\det \begin{pmatrix} \nu_s - G_m l^2 & \xi_1 & \xi_2 & \xi_3 \\ \nu_1 & \Gamma_1 & 0 & 0 \\ \nu_2 & 0 & \Gamma_2 & 0 \\ \nu_3 & 0 & 0 & \Gamma_3 \end{pmatrix} = 0, \tag{39}$$

where I have used the definition of α, equation 27. This can be seen by factoring out the identity matrices and the vectors $\mathbf{l}_1^\perp$ and writing the system 38 as four equations for the four unknowns t_s, t_1, t_2, and t_3. Alternatively, one can adopt the formal approach in Vasco and Minkoff (2012) and use the rule for the determinant of a matrix composed of block matrices (Silvester, 2000).

The vanishing of the determinant in equation 39 produces a quadratic equation for l with no linear term. I can solve the quadratic equation for l, resulting in the expression

$$l = \pm\sqrt{\frac{1}{G_m}\left(\nu_s - \frac{\xi_1\nu_1}{\Gamma_1} - \frac{\xi_2\nu_2}{\Gamma_2} - \frac{\xi_3\nu_3}{\Gamma_3}\right)}, \tag{40}$$

indicating a single solution for the transverse mode. The negative value signifies a wave propagating in the opposite direction. Because the other transverse vector $\mathbf{e}_2^\perp$ produces the same solution; both transverse waves propagate with the same speed. Making use of the definitions for ν_s and ν_i, I can write equation 40 in a more familiar form

$$l = \pm\omega\sqrt{\frac{(1-\phi)\rho_s - \phi\rho_f}{G_m}}, \tag{41}$$

where

$$\rho_f = \frac{\xi_1}{\Gamma_1}S_1\rho_1 + \frac{\xi_2}{\Gamma_2}S_2\rho_2 + \frac{\xi_3}{\Gamma_3}S_3\rho_3 \tag{42}$$

is a weighted fluid density. Note that the weights depend upon frequency through the ratios

$$\frac{\xi_i}{\Gamma_i} = \frac{\nu(1+\nu)^{-1}}{1-\nu(1+\nu)^{-1}}. \tag{43}$$

So the transverse slowness, or the corresponding wave speed, generally depends upon the frequency ω, perhaps leading to dispersive propagation. Furthermore, the ratio ξ_i/Γ_i can also be complex, leading to the attenuation of the transverse mode as it propagates.

The longitudinal modes of propagation

Now consider the situation in which the solid and fluid displacements are aligned with the direction of propagation $\mathbf{l}$. In such a case of longitudinal propagation, the eigenvector is of the form $\mathbf{e}^l$, given by equation 35. Therefore equation 34 is equivalent to

$$(\mathbf{A} - \hat{\mathbf{B}})\mathbf{e}^l = 0, \tag{44}$$

where $\mathbf{A}$ was given previously, equation 30, and

$$\hat{\mathbf{B}} = \begin{pmatrix} \beta l^2\mathbf{I} & C_{s1}l^2\mathbf{I} & C_{s2}l^2\mathbf{I} & C_{s3}l^2\mathbf{I} \\ C_{1s}l^2\mathbf{I} & M_{11}l^2\mathbf{I} & M_{12}l^2\mathbf{I} & M_{13}l^2\mathbf{I} \\ C_{2s}l^2\mathbf{I} & M_{21}l^2\mathbf{I} & M_{22}l^2\mathbf{I} & M_{23}l^2\mathbf{I} \\ C_{3s}l^2\mathbf{I} & M_{31}l^2\mathbf{I} & M_{32}l^2\mathbf{I} & M_{33}l^2\mathbf{I} \end{pmatrix}. \tag{45}$$

The matrix $\mathbf{A} - \hat{\mathbf{B}}$ consists of a 4×4 block matrix where each block contains the identity matrix, similar to the case for transverse propagation, equation 38. Following the procedure applied to that matrix, or the procedure described in Vasco and Minkoff (2012), I can show that the condition for equation 44 to have a nontrivial solution is the vanishing of the determinant of the matrix

$$\mathbf{M} = \begin{pmatrix} \nu_s - Hs & \xi_1 - C_{s1}s & \xi_2 - C_{s2}s & \xi_3 - C_{s3}s \\ \nu_1 - C_{1s}s & \Gamma_1 - M_{11}s & -M_{12}s & -M_{13}s \\ \nu_2 - C_{2s}s & -M_{21}s & \Gamma_2 - M_{22}s & -M_{23}s \\ \nu_3 - C_{3s}s & -M_{31}s & -M_{32}s & \Gamma_3 - M_{33}s \end{pmatrix}, \tag{46}$$

where I have defined

$$s = l^2 \tag{47}$$

and

$$H = K_u + \frac{4}{3}G_m. \tag{48}$$

The requirement that the determinant of the matrix $\mathbf{M}$ vanish results in a fourth-order polynomial for s. However, expanding the determinant using the standard formula (Noble and Daniel, 1977, p. 199) will result in complicated expressions for the coefficients of the polynomial. A better approach, presented in Vasco and Minkoff (2012), makes use of an expression for the determinant of a matrix in which a column is the sum of two components. For example, each term in the coefficient matrix $\mathbf{M}$ is composed of a constant term and a term linear in s. Thus, I can expand the determinant of the matrix $\mathbf{M}$ as

$$\det \mathbf{M} = \begin{vmatrix} \nu_s & \xi_1 - C_{s1}s & \xi_2 - C_{s2}s & \xi_3 - C_{s3}s \\ \nu_1 & \Gamma_1 - M_{11}s & -M_{12}s & -M_{13}s \\ \nu_2 & -M_{21}s & \Gamma_2 - M_{22}s & -M_{23}s \\ \nu_3 & -M_{31}s & -M_{32}s & \Gamma_3 - M_{33}s \end{vmatrix}$$
$$- s \begin{vmatrix} H & \xi_1 - C_{s1}s & \xi_2 - C_{s2}s & \xi_3 - C_{s3}s \\ C_{1s} & \Gamma_1 - M_{11}s & -M_{12}s & -M_{13}s \\ C_{2s} & -M_{21}s & \Gamma_2 - M_{22}s & -M_{23}s \\ \nu_3 & -M_{31}s & -M_{32}s & \Gamma_3 - M_{33}s \end{vmatrix}, \tag{49}$$

where the vertical bars signify that the quantity is the determinant of the enclosed matrix. I can apply this procedure recursively to produce the quartic equation

$$Q_4 s^4 - Q_3 s^3 + Q_2 s^2 - Q_1 s + Q_0 = 0 \tag{50}$$

with coefficients that are linear combinations of the determinants of 4×4 matrices, given in Appendix B. The quartic equation can be solved either numerically or analytically. An explicit solution can be derived in terms of the solutions of a related cubic equation, the resolvent cubic (Clark, 1984; Faucette, 1996; Stahl, 1997; Nickalls, 2009). Note that if Q_4 vanishes, then equation 50 reduces to a cubic equation with three roots. This can occur if any of the rows are proportional to one another. For example, if the mechanical properties of two of the fluids are similar then the seismic slowness would not be sensitive to the relative proportion of the two fluids. Effectively, there would be two seismically indistinct fluids in the pore space and the two-phase results of Vasco and Minkoff (2012) may be used.

The quartic equation 50 leads to a set of partial differential equations for the phase function $\theta(\mathbf{x}, \omega)$, introduced in equations 19 and 20. Each partial differential equation is a Hamilton-Jacobi equation for $\theta(\mathbf{x}, \omega)$, known as an eikonal equation (Chapman, 2004). The eikonal equations, and the equivalent characteristic equations may be used to define the trajectories or rays on which solutions are prescribed (Courant and Hilbert, 1962). Note that the trajectories are generally frequency-dependent and differ for each mode of propagation. There is a distinct phase variable associated with each mode, that is for each of the four roots of equation 50. To see this, consider equation 50 written in the factored form

$$(l^2 - s_1)(l^2 - s_2)(l^2 - s_3)(l^2 - s_4) = 0, \tag{51}$$

where the definition 47 has been used to substitute l^2 for s. From the definition 26 of $\mathbf{l}$ one can see that equation 51 is equivalent to

$$(\nabla\theta \cdot \nabla\theta - s_1)(\nabla\theta \cdot \nabla\theta - s_2)(\nabla\theta \cdot \nabla\theta - s_3) \times (\nabla\theta \cdot \nabla\theta - s_4) = 0. \tag{52}$$

Thus, each root produces an eikonal equation of the form

$$\nabla\theta \cdot \nabla\theta - s_i(\mathbf{x}, \omega) = 0,$$

where the dependence of the root s_i on the spatial coordinates, through the heterogeneity of the medium parameters has been made explicit, similarly for the frequency dependence.

APPLICATIONS

Here, I apply the methods presented above to three illustrative examples. In the first example, I compare the phase velocity estimates for the case in which one of the fluid saturations goes to zero, reducing the problem to that of two-phase flow. I compare the predictions made using the current methods to those made using the techniques described in Vasco and Minkoff (2012), which are in agreement with the earlier calculated values of Tuncay and Corapcioglu (1996) and Lo et al. (2005). In the second example, I consider the most general situation in which there are three fluids in the porous medium. For this case, there are four modes of longitudinal propagation and the velocities and attenuation coefficients vary as functions of the water, gas, and oil saturations. In the final example, I use the results of a compositional numerical simulation of the cyclic injection of water and carbon dioxide into a reservoir containing oil to examine the velocity variations induced by EOR.

Before tackling the individual modes of propagation, one needs to determine an expression for ν in terms of the properties of the medium. As stated in the discussion following equation 5, the quantity $(1 + \nu)^{-1}$ is referred to as the dynamic tortuosity (Johnson et al. 1987) and it is determined by the amount of fluid flowing in response to an applied force. Rather then enter into a detailed analysis of the physics of flow that might enable us to derive expressions for simplified media (Pride et al., 1993), I adopt a more pragmatic approach. That is, as in Vasco and Minkoff (2012), I determine a value for ν by comparing the appropriate coefficients in the governing equations 15 and 16 with the governing equations in Tuncay and Corapcioglu (1996). In particular, after transforming their equations into the frequency domain and accounting for a somewhat different formulation, I have

$$\xi_j = -i\omega C_j \tag{53}$$

and

$$\Gamma_j = \omega^2 \hat{\rho}_j + i\omega C_j \tag{54}$$

for $j = 1, 2, 3$, where C_j are the coefficients in Tuncay and Corapcioglu (1996) augmented by the additional fluid phase, of the form

$$C_j = \frac{\phi^2 S_j \mu_j}{k k_{rj}} \tag{55}$$

for Darcy flow, and $\hat{\rho}_j$ is the volume averaged density, given by $\hat{\rho}_j = \alpha_j \rho_j = \phi S_j \rho_j$. Recall the flow properties contained in C_j: the porosity ϕ, the absolute permeability k, and the relative permeability for fluid j, k_{rj}. Using equations 53, and the equations represented by 11, I can solve for an explicit expression for ν:

$$\nu = \frac{C_j}{C_j + i\omega\alpha_j\rho_j}. \tag{56}$$

Note that ν appears to be a function of the particular fluid of interest and that it is a frequency-dependent, complex quantity. Using this expression for ν, and the expressions 55 for C_j, I can calculate all the coefficients of the governing equations in terms of the properties of the fluids and the properties of the medium. Thus, I can define all the parameters in the expressions 41 and 50 determining the slownesses for the transverse and longitudinal modes of propagation.

For the transverse and longitudinal modes, there is the issue of calculating the relative permeabilities for a porous medium containing three fluid phases. This is not a trivial undertaking and is the subject of a significant amount of research that I can only touch upon. The earliest work was that of Leverett and Lewis (1941) on unconsolidated sands. An influential model was developed by Stone (1973) and subsequently modified by Aziz and Settari (1979). In their approach, the three-phase relative permeability model is constructed from sets of two-phase observations. Corey et al. (1956) estimated three-phase relative permeabilities based upon simple measurements of saturation pressure data. Other influential models include those of Baker (1988), Jerauld (1997), and Blunt (2000). Many of the models assume that the relative permeability of the gas phase only depends upon the gas saturation, and similarly for the aqueous phase, whereas the relative permeability of the oil phase is a function of the gas and aqueous saturations. A model by Sarem (1966) assumed that the relative permeabilities only depended on the saturation of each phase in question.

Here, I use the three-phase relative permeability functions of Parker et al. (1987), generalizations of the two-phase formulation of Van Genuchten (1980) and Mualem (1976). The exact form of the relative permeability functions are

$$k_{rg} = \sqrt{\bar{S}_g}[1 - (\bar{S}_l)^{1/m}]^{2m} \tag{57}$$

$$k_{rw} = \sqrt{\bar{S}_w}\{1 - [1 - (\bar{S}_w)^{1/m}]^m\}^2 \tag{58}$$

$$k_{ro} = \sqrt{\bar{S}_l \bar{S}_w}\{[1 - (\bar{S}_w)^{1/m}]^m - [1 - (\bar{S}_l)^{1/m}]^m\}^2 \tag{59}$$

for the gas, water, and oil phases, respectively, where

$$\bar{S}_g = \frac{S_g}{1 - S_m} \tag{60}$$

$$\bar{S}_w = \frac{S_w - S_m}{1 - S_m} \tag{61}$$

$$\bar{S}_l = \frac{S_w + S_o + S_m}{1 - S_m} = \frac{1 - S_g + S_m}{1 - S_m}, \tag{62}$$

where $m = 1 - 1/n$ is an exponent and S_m is an apparent minimum or irreducible wetting fluid saturation. As in many of the other formulations, the gas and aqueous relative permeabilities only depend upon their respective saturations, whereas the oil relative permeability depends upon the gas and water saturations. In Figure 1, I plot the water, gas, and oil relative permeabilities for a model that is similar to the two-phase relative permeability functions used in Vasco and Minkoff (2012) with $n = 2.037$ and $S_m = 0.0$.

Prior to entering into detailed calculations and comparisons of the various prediction, I wish to take a step back and consider the fundamental parameters required for the computations. There are 12 essential quantities, indicated in Table 1, which all the computations depend upon. The 12 properties can be grouped into three main categories as indicated in the table and mentioned in the Methodology section. The parameter values used in the calculations involving two and three fluids and in the simulation of the injection of carbon dioxide are also given in Table 1. The parameters used in the two- and three-phase test calculations were chosen to facilitate a comparison with two previous studies. In particular, as in the previous two-phase work of Vasco and Minkoff (2012), the values from Lo et al. (2005) were used to allow for a qualitative comparison with their results. A computer program containing the explicit expressions for the coefficients presented in Tuncay and Corapcioglu (1996) allowed for a quantitative comparison with their two-phase predictions, as in Vasco and Minkoff (2012). Because Lo et al. (2005) were modeling an unconsolidated Columbia fine sandy loam, the frame moduli are significantly smaller then typical reservoir rocks (Table 1). Thus, one would expect that the velocities would be lower then those usually observed in a deep reservoir.

A comparison with two-phase estimates

The comparison of the three-phase estimates with previous two-phase estimates (Vasco and Minkoff, 2012) is done in two stages. First, I consider transverse displacements that have a relatively simple relationship to the medium properties through equations 39 and 41. The dependence of the transverse slowness on the flow properties of the porous medium is through the ratio ξ_i/Γ_i, which depends upon ν as shown in equation 43. As shown above, assuming Darcy flow, the quantity ν depends upon the porosity, the intrinsic permeability k, and the relative permeabilities k_{ri}. The slowness of the transverse displacement does not depend upon the capillary pressure variation of the porous medium.

Transverse displacements

Now consider the expression for the phase velocity of the transverse mode of propagation. As noted in Vasco and Minkoff (2012), due to the particular definition of the phase function θ, the phase velocity, c, is given by

$$c = \frac{\omega}{l} \tag{63}$$

where l is given by equation 41.

To compare the three-phase velocity estimates to two-phase estimates using the approach described in Vasco and Minkoff (2012),

consider the case in which one of the saturations vanishes. For example, if the gas phase vanishes then the problem reduces to a two-phase system, consisting of oil and water. In that case, the relative permeability curves are given by equations 57, 58, and 59 with one of the saturations S_w, S_g, or S_o set equal to zero. In essence, one is using the relative permeability variations from pairs of edges of the triangles shown in Figure 1. The resulting phase velocity estimates, as a function of the water saturation, are shown in Figure 2 for oil-water and gas-water systems. The two-phase estimates are indicated by the symbols whereas the three-phase estimates are denoted by the dashed lines. The estimates were computed at a frequency of 100 Hz. In Figure 3, I plot the velocity estimates for a gas-water system over a range of frequencies. Velocity estimates are shown for water saturations of 0.1 and 0.9.

Longitudinal displacements

The velocities associated with the longitudinal modes of displacement are determined by solutions of the quartic polynomial 50. The coefficients of the polynomial depend upon the parameters in the governing equations 15 and 16. For a Biot model, the parameters are given in Appendix A. There, I show that the capillary properties of the medium influence the velocities of the longitudinal modes. This was not the case for the transverse mode of displacement. The capillary pressure functions that I use are those of Parker et al. (1987)

$$P_{\rm cgo} = -\frac{\rho_w g}{\alpha_{go}}[\bar{S}_l^{-1/m} - 1]^{1/n} \tag{64}$$

$$P_{\rm cgw} = -\frac{\rho_w g}{\alpha_{ow}}[\bar{S}_w^{-1/m} - 1]^{1/n} - \frac{\rho_w g}{\alpha_{go}}[\bar{S}_l^{-1/m} - 1]^{1/n}, \tag{65}$$

plotted in Figure 4 along with $P_{\rm cow} = P_{\rm cgo} - P_{\rm cgw}$. As I did for the transverse mode of displacement, to compare the three-phase estimates with two-phase estimates (Vasco and Minkoff, 2012), I shall consider cases in which one of the fluid saturations vanishes.

First, consider the gas-water system in which the oil saturation is zero. In Figure 5, I plot the gas-water capillary pressure, $P_{\rm cgw}$ variation using the curve given by equation 65 and the two-phase capillary pressure model of Van Genuchten (1980) used by Vasco and Minkoff (2012). In this case, the two curves differ; the model of Parker et al. (1987) is different from the two-phase Van Genuchten (1980) model. In Figure 6, the longitudinal velocities $P1$, $P2$, and $P3$ estimates, made using the method described above, are plotted along with the two-phase estimates based upon the two-phase formulation of Vasco and Minkoff (2012). The fast wave ($P1$) velocities are identical for the three-phase and two-phase estimates, regardless of the difference in the capillary pressure curves. The other two velocities, $P2$ and $P3$, appear to be strongly influenced by the difference in the capillary pressure curves.

Next, consider the case in which the gas phase vanishes and I have an oil-water system. The capillary pressure curves computed using the two-phase (Van Genuchten, 1980) and the three-phase (Parker et al., 1987) formulations are shown in Figure 7. In this case, the two-phase and three-phase capillary pressure curves differ to a lesser degree. The three longitudinal velocities, $P1$, $P2$, and $P3$ are shown in Figure 8, computed using the two- and three-phase

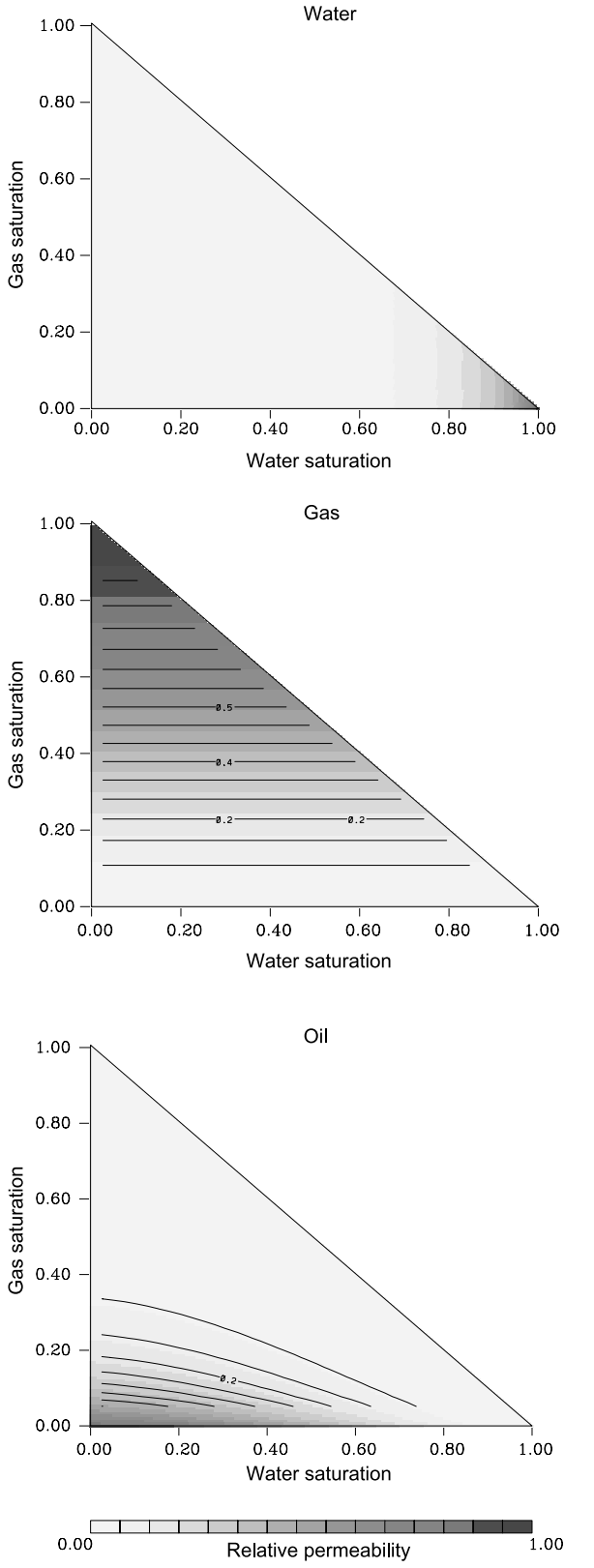

Figure 1. Three-phase relative permeability functions, k_{rw} (top), k_{rg} (middle), and k_{ro} (bottom) of Parker (1987), as given by equations 58, 57, and 59. The relative permeabilities are plotted as functions of the water and gas saturations which are the two independent saturations because $S_o = 1 - S_w - S_g$.

approaches. Again, the fast velocities $P1$ agree for both approaches whereas the other two velocity estimates ($P2$ and $P3$) differ, though to a lesser degree than for the gas-water system.

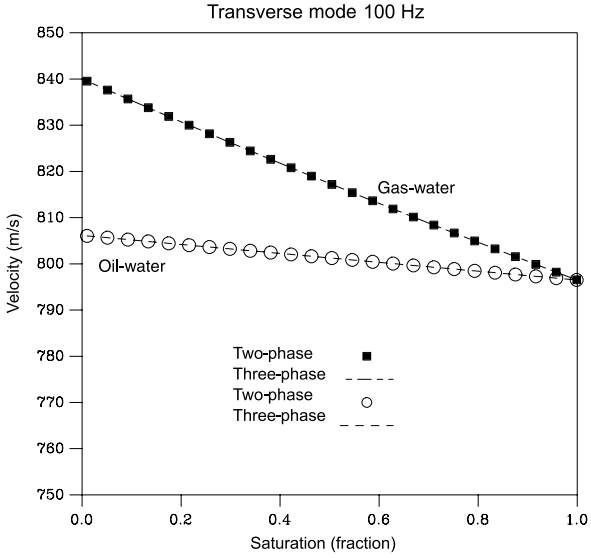

Figure 2. Phase velocity of the transverse mode of displacement as a function of the water saturation, S_w. The center frequency of the disturbance is 100 Hz. There are two distinct cases plotted here: only gas and water are present (gas-water), and only oil and water are present (oil-water). The symbols (filled squares and open circles) denote the velocities computed using the two-phase approach of Vasco and Minkoff (2012). The dashed lines denote the velocity estimates made using the approach described in the text of this paper.

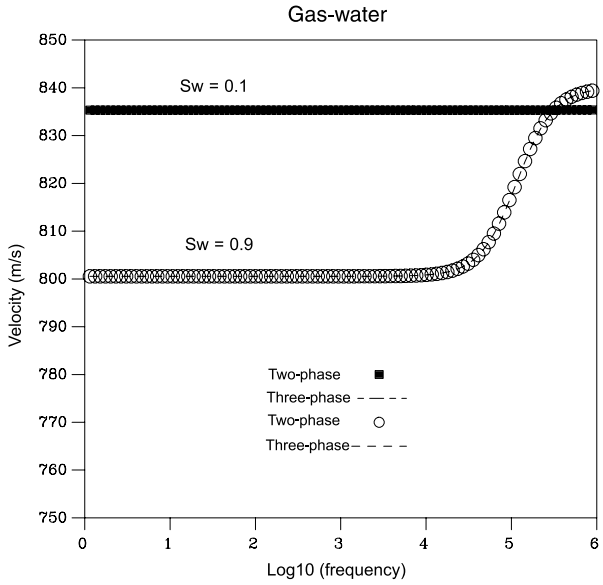

Figure 3. Phase velocity as a function of the frequency in hertz for a system in which only gas and water are present. Two distinct water saturations are considered, $S_w = 0.1$ and $S_w = 0.9$. As in Figure 2, the symbols denote the two-phase estimates of Vasco and Minkoff (2012) whereas the dashed lines denote the three-phase estimates.

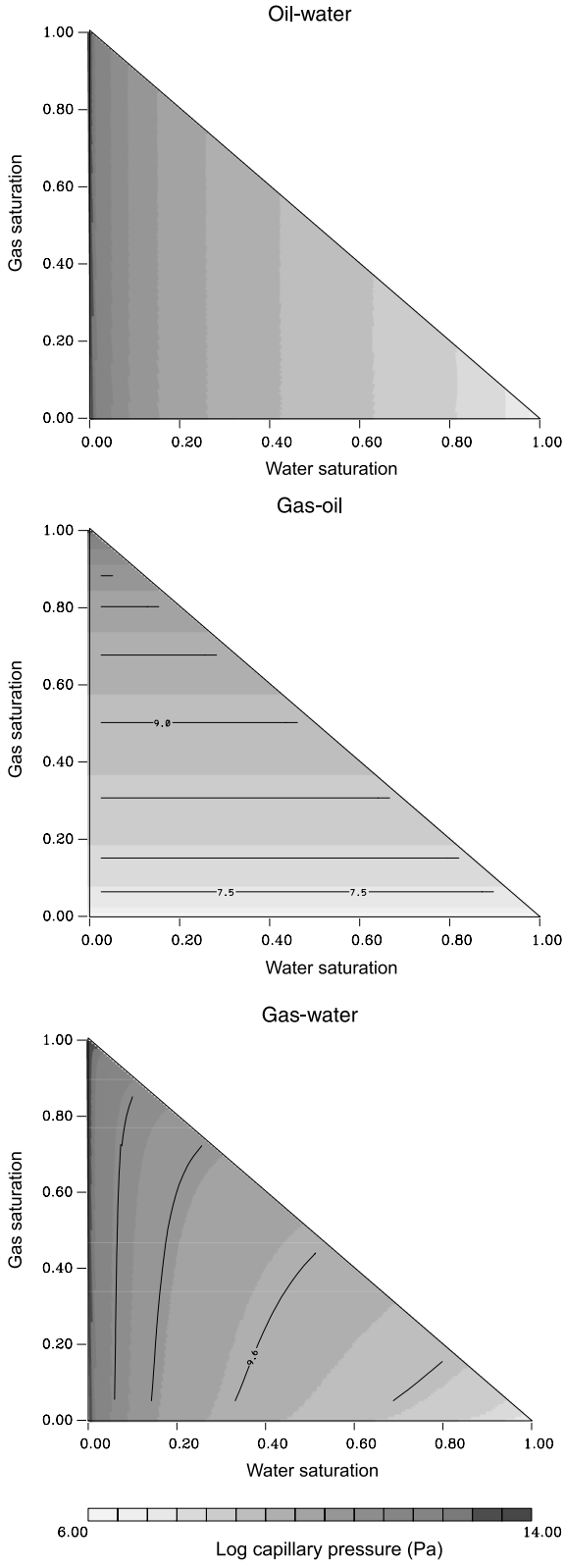

Figure 4. Capillary pressure curves of Parker (1987), given by equations 64 and 65, as functions of the water and gas saturation. Of the three capillary pressure functions, P_{cow} (top), P_{cgw} (middle), and P_{cgw} (bottom) only two are independent because $P_{\mathrm{cow}} = P_{\mathrm{cgo}} - P_{\mathrm{cgw}}$.

In the presence of three fluid phases

Now consider the situation in which three fluids are present in the porous medium. The relative permeability (equations 57–59) and capillary pressure (equations 64 and 65) functions of Parker et al. (1987) are used in the calculations. The solid, fluid, and flow parameters are given in Table 1.

Transverse displacements

For transverse displacements, there is only a single mode of propagation, though this mode will have two degrees of freedom in the plane transverse to the direction of propagation. The range of the transverse velocity over all possible three-phase fluid saturations is shown in Figure 9. As hinted at by the linear variations in Figure 2, at a frequency of 100 Hz the velocity of the transverse mode appears to be a linear function of the fluid saturations. Note that this is not true at all frequencies, as indicated in the lower panel of Figure 9 where I plot the velocities for a frequency of 50 KHz. Such behavior is suggested by the high-frequency variation of the transverse mode velocities in Figure 3. In particular, the phase velocities for the high and low saturations appear to cross over as the frequency is increased to a sufficiently high value.

Longitudinal displacements

Consider the situation in which the displacement is in the direction of propagation **l**. In this case, there are four solutions to the quartic equation 50 and hence four modes of longitudinal propagation. The velocities associated with the four longitudinal modes are functions of the three fluid saturations. Therefore, one must plot the velocities as functions of the three fluid saturations, constrained by the fact that the saturations sum to unity (see equation 1). Thus, it is best to plot the velocities over phase triangles as in Figure 10. In these plots, the origin, which signifies that no water or gas are present, represents the case in which the medium is entirely saturated

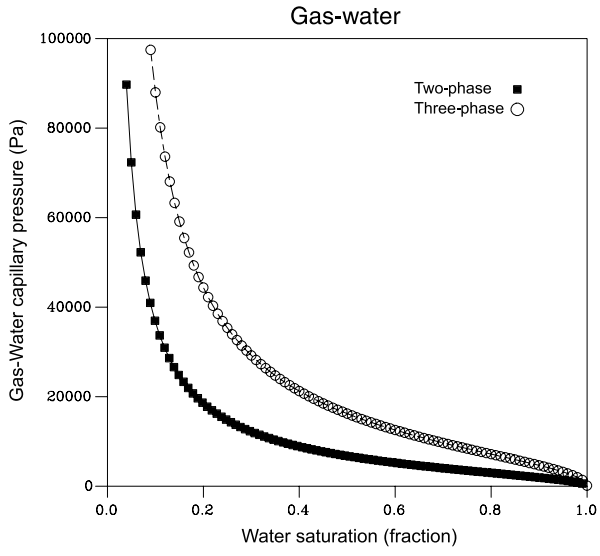

Figure 5. Relative permeability curves for the gas-water system ($S_o = 0$), for the capillary pressure function P_{cgw}. The two-phase capillary pressure curve is that of van Genuchten (1980) whereas the three-phase curve is from Parker (1987).

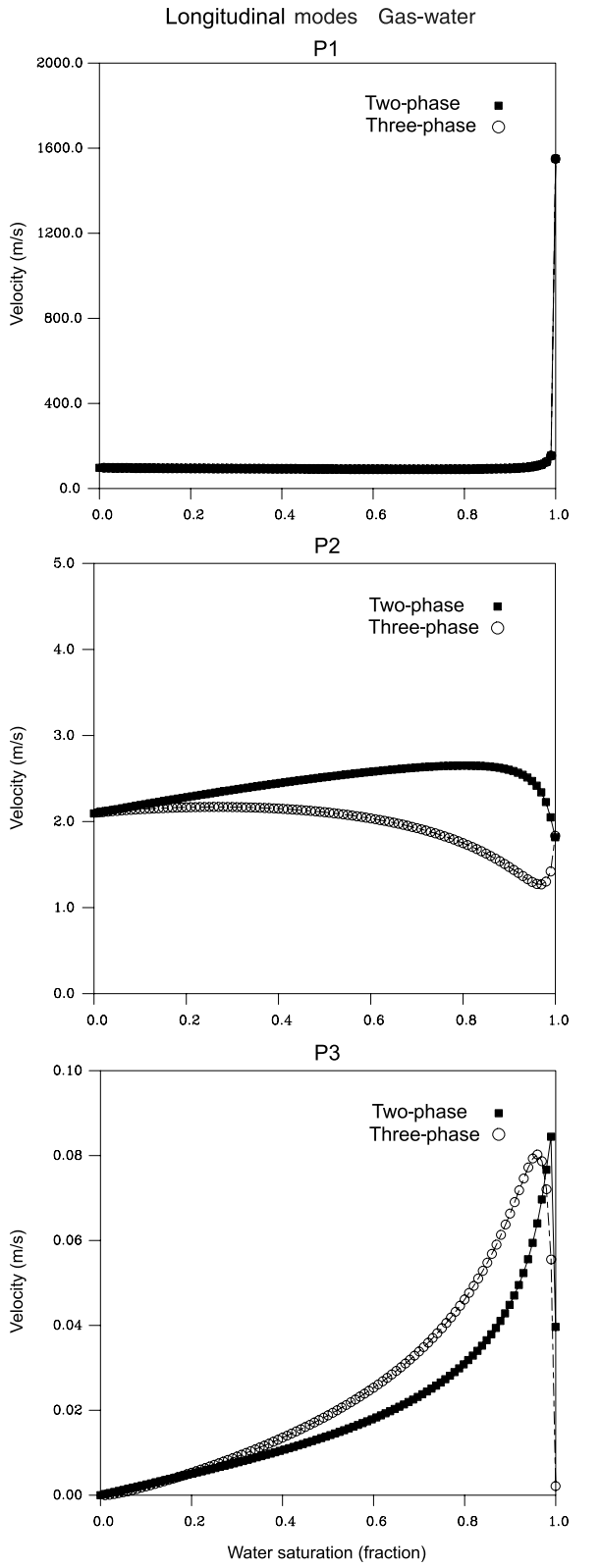

Figure 6. The first three longitudinal phase velocities for the gas-water system (vanishing S_o) as a function of the water saturation. The two-phase estimates are denoted by the filled squares whereas the three-phase estimates are indicated by the open circles.

with oil. The diagonal of the triangle is the line on which no oil is present, thus signifying a pure gas-water system.

The complete set of velocity estimates, for each of the phase triangles, are shown in Figure 10. As is evident from the coefficients 9, 10, 11, and 12 the velocities are frequency-dependent, and for this example are computed for a frequency of 100 Hz. As indicated in Figure 6, and noted by others, the presence of even a small amount of gas has a dramatic effect on the velocity of the fastest longitudinal mode ($P1$). Thus, for $P1$ the velocity is low, around 100 m/s for most of the saturation triangle and only approaches much higher values (more than 1500 m/s), when the gas saturation is less then 1%. The velocity variation of the second longitudinal mode ($P2$) is also dominated by the gas saturation until S_g is less than 5%–10%. However, the velocity associated with this mode is generally higher for larger gas saturations. This may be due to the lower viscosity of gas compared to the viscosities of oil and water. The longitudinal mode corresponding to $P2$ is similar to a diffusive transient pressure disturbance and is strongly influenced by the flow properties and the fluid properties (Pride, 2005; Vasco, 2009). For the lower values of the gas saturation, the $P2$ velocity has a minimum between water saturations of 0.6 and 0.9, in agreement with the variation plotted in Figure 8. The velocity variations for the $P3$ and $P4$ longitudinal modes are the most complicated, perhaps due to its sensitivity to the capillary pressure differences between the fluid phases. In contrast to $P2$, the highest velocities for $P3$ and $P4$ occur when the gas saturation is a minimum.

In general, the solutions, or roots, of the quadratic equation 50 are complex. The attenuation coefficient is the imaginary component of l, and is given by the imaginary component of the root. Due to the nature of the contribution of the phase θ to the displacements (see equations 19 and 20) a positive imaginary component represents exponential decay as the disturbance propagates. A larger imaginary component signifies much greater attenuation for a given propagation distance. In Figure 11, the attenuation coefficients are plotted as functions of the water, gas, and oil saturations.

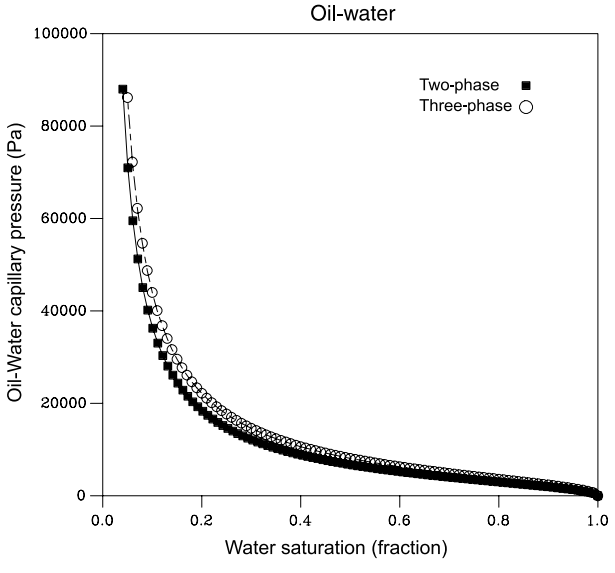

Figure 7. Relative permeability curves for the oil-water system (vanishing S_g), for the capillary pressure function P_{cow}. The two-phase capillary pressure curve is that of van Genuchten (1980), whereas the three-phase curve is from Parker (1987).

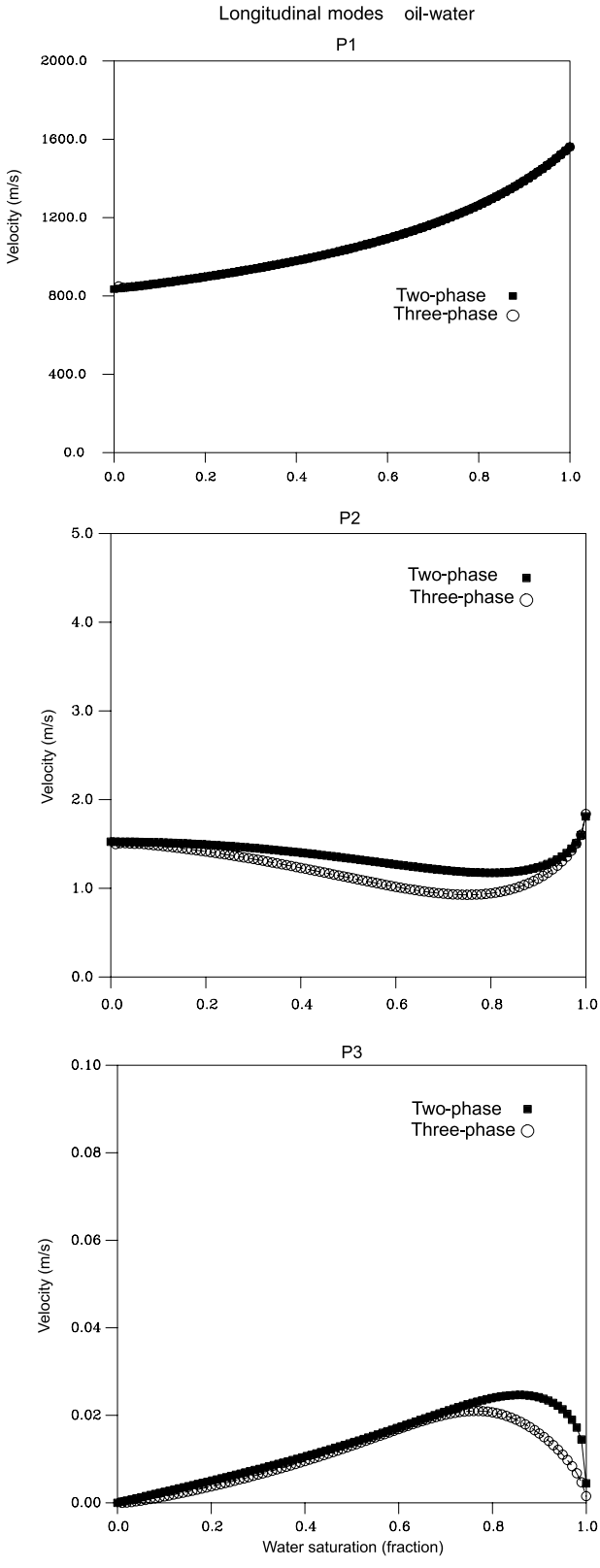

Figure 8. The first three longitudinal phase velocities for the oil-water system (vanishing S_g) as a function of the water saturation. The two-phase estimates are denoted by the filled squares whereas the three-phase estimates are indicated by the open circles.

The attenuation coefficient associated with $P1$ is quite small, less than 0.001 m^{-1}. The largest values occur when the gas saturation is around 10% and for higher values of water saturation. For the second mode ($P2$), the attenuation coefficient is at least five orders of magnitude larger, with a peak value of around 400 m^{-1}. The attenuation is greatest for very low gas saturations and water saturations of around 0.6 to 0.8, the same region in which the phase velocity is low (Figure 10). The attenuation coefficients for the $P3$ and $P4$ longitudinal modes are roughly three orders of magnitude larger then that for $P2$. They are largest for high gas saturations and are generally inversely related to the phase velocities shown in Figure 10. In general, the modes $P3$ and $P4$ and severely attenuated as they propagate, indicating that they will be difficult to observe.

As noted above, the coefficients, and hence the roots of the quadratic equation 50 are frequency-dependent and we would expect that the phase velocities and the attenuation coefficients to be functions of frequency. To view the frequency-dependence, I fix the fluid saturations at equal values, that is at $S_w = S_o = S_g = 1/3$, and allow the frequency to vary from 1 Hz to 10^5 Hz (Figure 12). In general, the fastest velocity, $P1$, does not change significantly over the frequency band, which encompasses the seismic frequency range. The velocity associated with the $P2$ mode, which is similar to a transient fluid pressure disturbance, changes significantly from about 100 Hz onward. Similarly, the two modes associated with capillary pressure differences, $P3$ and $P4$ have velocities that increase rapidly after 10 to 100 Hz. Such behavior has been noted in other studies. For example, Tuncay and Corapcioglu (1996) plotted the phase velocities of $P1$, $P2$, and $P3$ for the situation in which two fluid phases are present. They recovered behavior similar to that shown in Figure 12, with increasing velocities for frequencies exceeding 100 Hz. Lo et al. (2005, 2009), who plotted phase velocities for waves propagating in a medium containing two fluids, give results for four frequencies (50, 100, 150, and 200 Hz). The general trend is one of increasing velocities with increasing frequency, as indicated in Figure 12.

In Figure 13, the attenuation coefficients of the four modes ($P1$, $P2$, $P3$, and $P4$) are plotted as functions of frequency. Again, I fix the fluid saturations at equal values, that is at $S_w = S_o = S_g = 1/3$, and allow the frequency to vary from 1 to 10^5 Hz. The behavior of the attenuation coefficient mirrors that of the phase velocity, increasing as a function of frequency. In general, the attenuation coefficient for the fastest mode, $P1$, increases at much higher frequencies, greater than 10^4 Hz, than do the coefficients for the other modes. For these modes ($P2$, $P3$, and $P4$), the attenuation starts to increase significantly at around 100 Hz. Neither Tuncay and Corapcioglu (1996) nor Lo et al. (2005, 2009) plot the attenuation coefficients as functions of frequency for their two-phase calculations. However, their plots of attenuation coefficients for various frequencies do display a similar trend: larger attenuation coefficients at higher frequencies.

Seismic velocity variations due to the injection of carbon dioxide

EOR is one area in which three fluid phases are likely to be present within a given reservoir. One particular technique that also serves to mediate greenhouse gas emissions involves injecting carbon dioxide to enhance secondary recovery. Depleted oil and gas fields are likely to contain two or more phases, such as oil and water or oil and gas. Injecting an additional phase, such as carbon dioxide will likely results in three-phase flow within the reservoir. Time-lapse seismic surveying has been proposed as a tool for monitoring the injection of carbon dioxide into oil and gas reservoirs as well as saline aquifers (Hoversten et al., 2003; Carcione et al., 2006; Kazemeini et al., 2010). In fact, time-lapse seismic observations are providing useful information regarding the migration of carbon dioxide within a reservoir (Arts et al., 2004). Thus, the injection of carbon dioxide provides a useful illustration of this approach for computing velocities in a poroelastic medium containing three fluid phases.

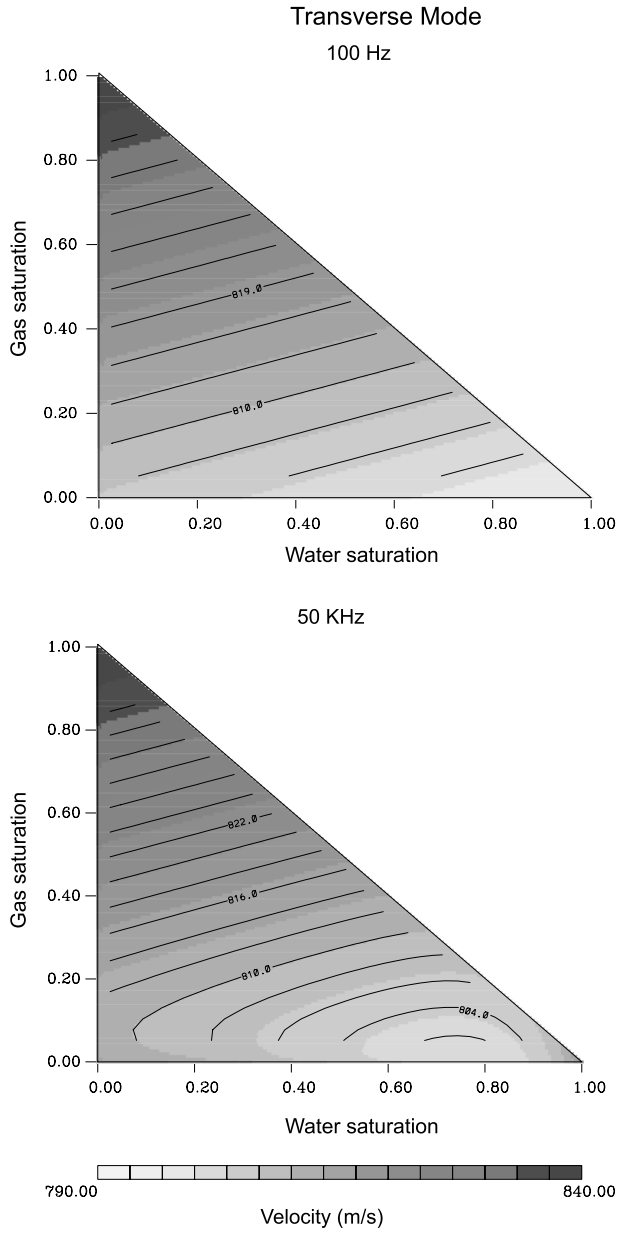

Figure 9. The phase velocity of the transverse mode of displacement as a function of the water and gas saturation. At the origin, where S_w and S_g are zero, the medium is fully saturated by oil. On the diagonal line, S_o vanishes and one has a gas-water system. (Top) Velocities for a frequency of 100 Hz. (Bottom) Velocities for a frequency of 50,000 Hz.

The illustration is based upon the Society of Petroleum Engineers' fifth comparative problem (Killough and Kossack, 1987) which simulates a water-alternating-gas production cycle. In this problem, water and carbon dioxide are injected into an oil saturated reservoir in a cyclic fashion over a span of 5479 days. The process was modeled using the Eclipse compositional reservoir simulator for three-phase flow (oil, water, and gas) with multiple components (C1N2, CO_2, C2, H_2S, C3C5, C6C11, C16P, C43P) allowed in the oil and gas phases (Schlumberger, 2005). The reservoir model consisted of three layers with each layer subdivided into a 7 × 7 grid of rectangular cells. The grid blocks are 152 × 152 m laterally and the layer boundaries are 2537.5, 2543.6, 2552.7, and 2567.9 m. The porosity in each layer is 0.3 and the permeabilities of the layers are 500, 50, and 200 millidarcies. The well configuration consists of

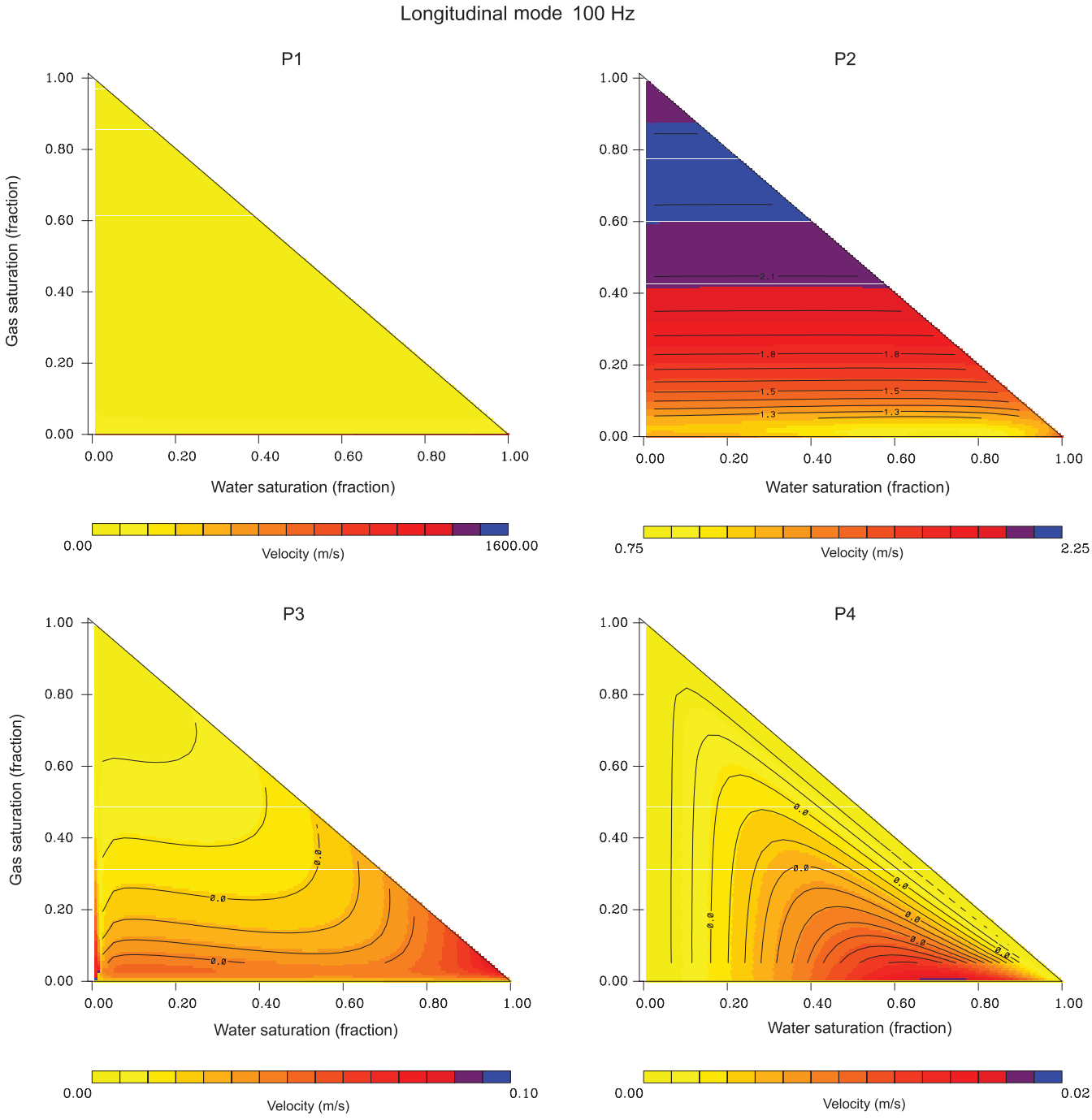

Figure 10. The four longitudinal phase velocities plotted as functions of the two independent saturations (S_w and S_g). At the origin, where S_w and S_g are zero, the medium is fully saturated by oil. On the diagonal line, S_o vanishes and one has a gas-water system. For the fast longitudinal model, $P1$, the velocities increase rapidly near the water saturation axis.

a quarter five-spot, as shown in Figure 14, with an injector in the lower left corner and a producer in the upper right corner. A cyclic injection of water, alternating with carbon dioxide, with a period of one year is modeled using the Eclipse 3000 multicomponent reservoir simulator (Schlumberger, 2005). The fluid pressure within the second layer, after 1096 days of injection, is shown in Figure 14, along with the flow trajectories from the injector to various locations within the model.

For multicomponent fluids, the densities, viscosities, and compressional moduli are functions of the chemical components in the fluids as well as functions of the fluid pressure and temperatures (Peaceman, 1977, p. 26). For a real fluid, the Peng-Robinson

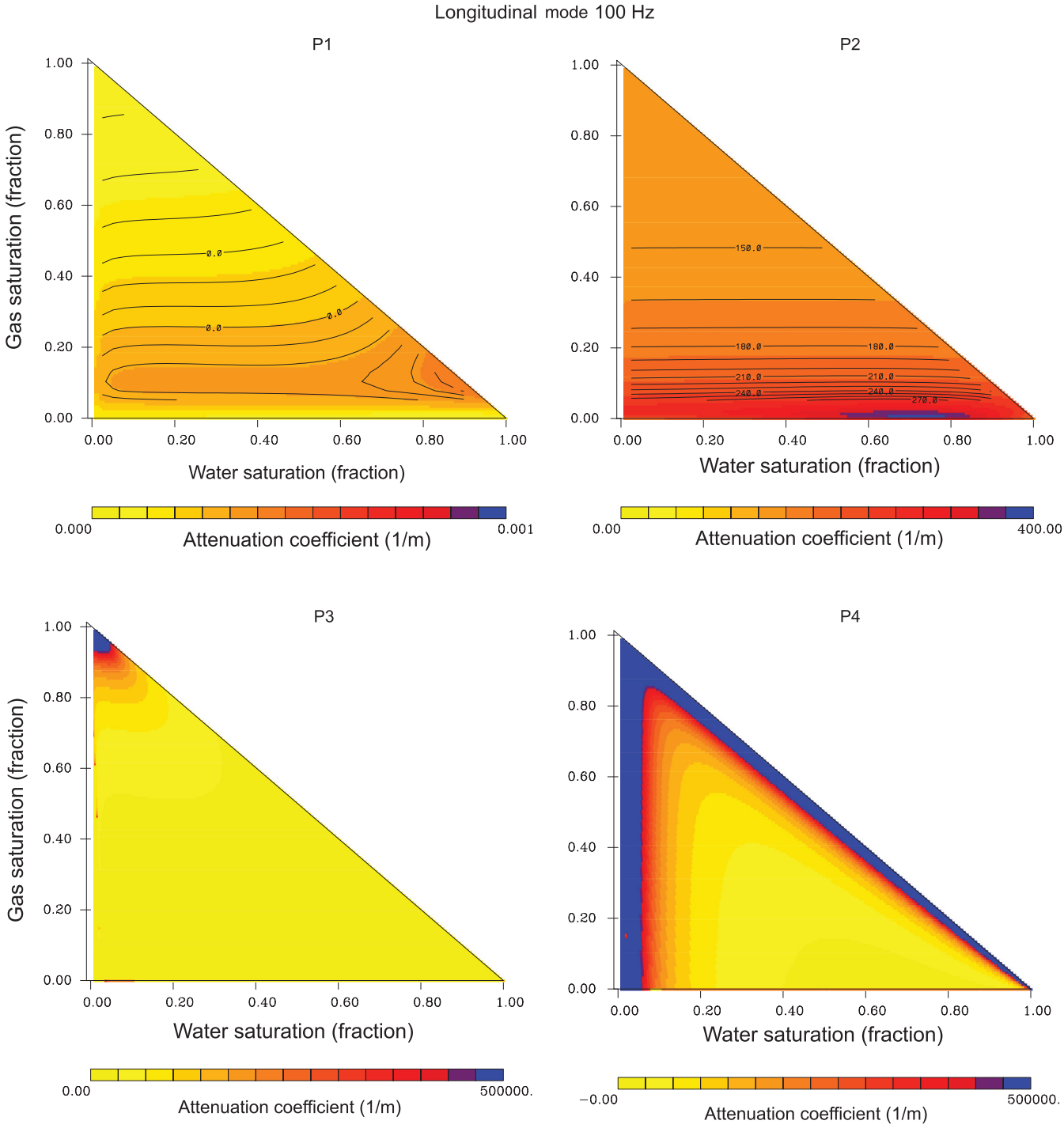

Figure 11. The four longitudinal attenuation coefficients, the imaginary component of the roots of the quadratic equation 50, plotted as functions of the two independent saturations (S_w and S_g). At the origin, where S_w and S_g are zero, the medium is fully saturated by oil. On the diagonal line, S_o vanishes and one has a gas-water system.

Figure 12. The phase velocities for the four longitudinal modes ($P1$, $P2$, $P3$, and $P4$) plotted as functions of frequency (Hz). For these calculations, I have considered the situation in which the fluid saturations are equal ($S_w = S_o = S_g = 1/3$).

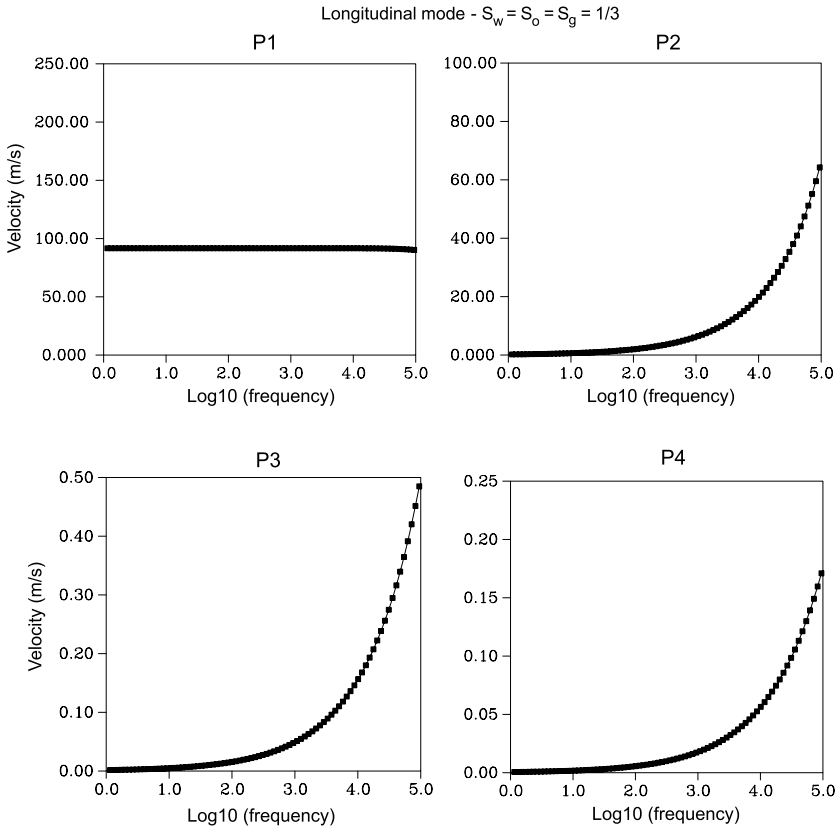

Figure 13. The attenuation coefficients for the four longitudinal modes plotted as functions of frequency (Hz). For these calculations, I have considered the situation in which the fluid saturations are equal ($S_w = S_o = S_g = 1/3$).

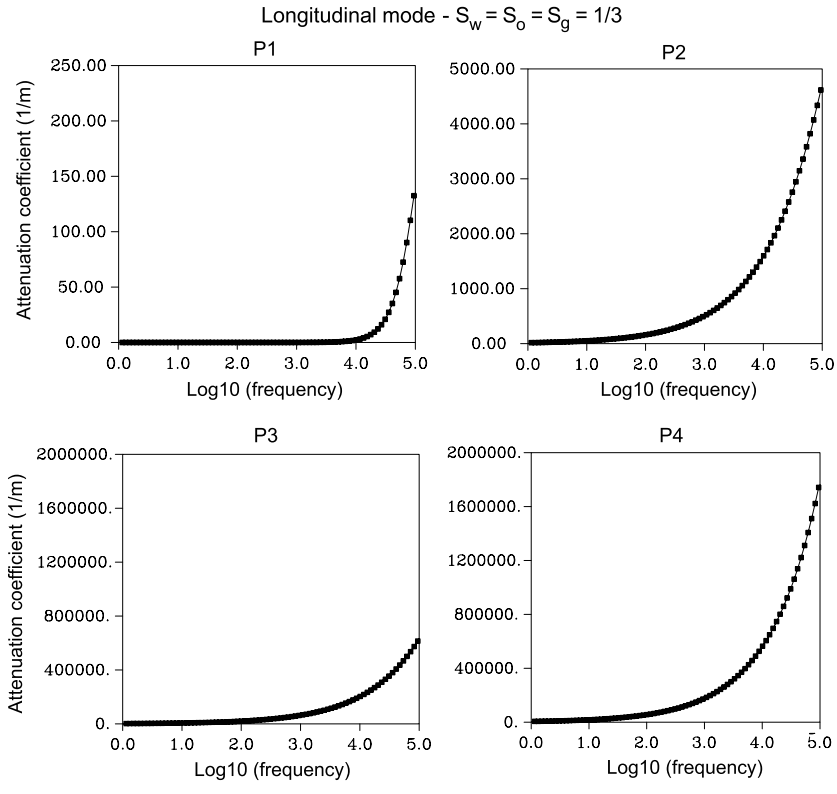

equation of state (Peng and Robinson, 1977), a generalization of van der Waals equation, is often used to relate the pressure (P) in the fluid component to the temperature (T) and volume (V)

$$P = \frac{RT}{V-b} - \frac{a}{[V+(\sqrt{2}+1)b][V-(\sqrt{2}-1)b]}, \quad (66)$$

where R is the gas constant and a and b are parameters characterizing the particular fluid component. For a multicomponent mixture, the coefficients are defined in terms of the concentrations X_i, and the parameters of the individual component, a_i and b_i, according to

$$a = \sum_i \sum_j X_i X_j (1-\delta_{ij}) \sqrt{a_i} \sqrt{a_j} \quad (67)$$

$$b = \sum_i X_i b_i, \quad (68)$$

where δ_{ij} are empirically determined interaction coefficients (Peng and Robinson, 1977). The details of the multicomponent modeling, including modifications to the Peng-Robinson equation of state, may be found in the Eclipse manual (Schlumberger, 2005). It should be noted that there are newer equations of state that may better represent mixtures of hydrocarbon chains (Wei and Sadus, 2000; Marghari and Hosseinzadeh-Shahri, 2003). The simulator partitions the chemical components among the three fluid phases and calculates the composite properties of each phase. In particular, the numerical simulator outputs the viscosities and densities of each phase directly.

In addition to the viscosities and densities, one also requires the bulk modulus of each fluid phase to compute the velocities (see the matrix **K** given by the expression A-25). The bulk modulus of each phase may be derived from the equation of state using the definition of the isothermal bulk modulus

$$K_T = -V \frac{\partial P}{\partial V}, \quad (69)$$

where the derivative is evaluated at a specific constant temperature. An explicit expression for K_T follows from Peng-Robinson equation of state 66

$$K_T = V \frac{RT}{(V-b)^2} - \frac{2aV(V+b)}{(V^2+2bV-b^2))^2}. \quad (70)$$

To obtain the adiabatic bulk moduli, the quantity associated with elastic wave propagation, and the corresponding quantities for the three fluid phases (K_1, K_2, and K_3 in equation A-14), one must multiply the expression 70 by the ratio of the specific heat capacities (Batzle and Wang, 1992). As noted by Batzle and Wang (1992), the ratio of the specific heat capacities can be expressed in terms of the equation of state of the fluid and a reference curve of the constant pressure heat capacity.

The water, oil, and gas phase saturations and the phase densities and viscosities calculated by the numerical simulator are used in computing the coefficients in the governing equations 15 and 16. The water, gas, and oil saturations in the second layer, 1096 days after the start of injection, are shown in Figure 15. A bank of water is visible in the lower left corner of the model as is the gas due to two cycles of carbon dioxide injection. There is also gas present around the producer, perhaps due to the production-induced pressure decrease, causing gas to come out of solution.

Using the output of the numerical simulator, along with the relative permeability and capillary pressure functions of Parker et al. (1987) described earlier (see equations 57, 58, 59, 64, and 65), I constructed the coefficients for equations 41 and 50 defining the slownesses of the transverse and longitudinal modes of displacement. The properties of the solid grains are: $\rho_s = 2650$ kg/m^3 and $K_s = 34.0$ GPa, those of the frame are: $K_{fr} = 1.5$ GPa and $G_{fr} = 1.0$ GPa (Table 1). A frequency of 100 Hz was used in the calculations. For the velocity of the transverse mode (Figure 16), the most significant feature is a region of low velocity corresponding to the bank of water. This agrees with the variation plotted in Figure 9 which indicates that the lowest velocity of the transverse mode of propagation at 100 Hz occurs when the water saturation is greatest. Conversely, for the fastest longitudinal model (P1), one observes relatively higher velocities associated with the water bank and low velocities associated with the areas of greatest gas saturation (Figure 17). The peak velocity variations are around 10% of the background velocity of 1600 m/s. Such velocity variations are of the same order as those observed in laboratory experiments involving the injection of carbon dioxide into a water saturated sandstone at a pressure of 12 MPa (Shi et al., 2007). The second phase velocity, $P2$, appears to be greatest where the gas saturation is highest, in agreement with the behavior shown in Figure 10.

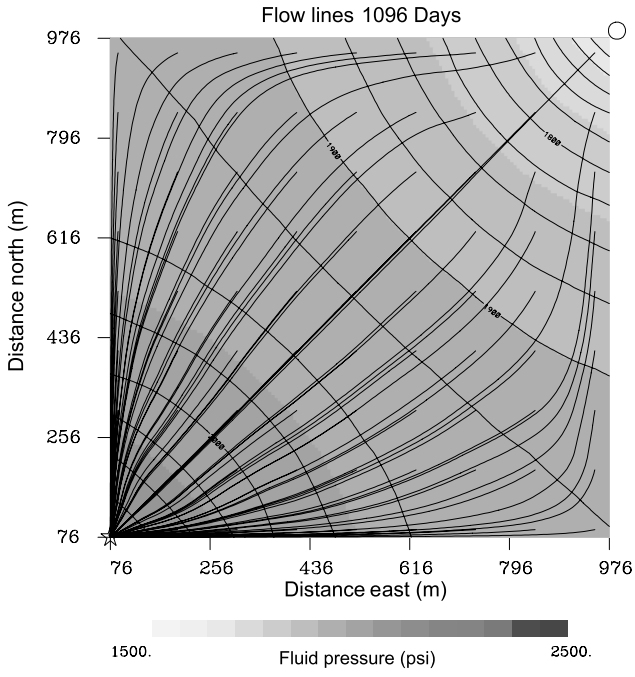

Figure 14. Fluid pressure variations associated with a numerical simulation of a cyclical water alternating gas injection. The water and gas are alternatively injected in yearly cycles. The pressure shown is after 1096 days of injection. The fluid flow lines are plotted in this figure, extending from the injection well (open star) to various points in the reservoir layer. The production well is indicated by the open circle in the upper right corner of this plot.

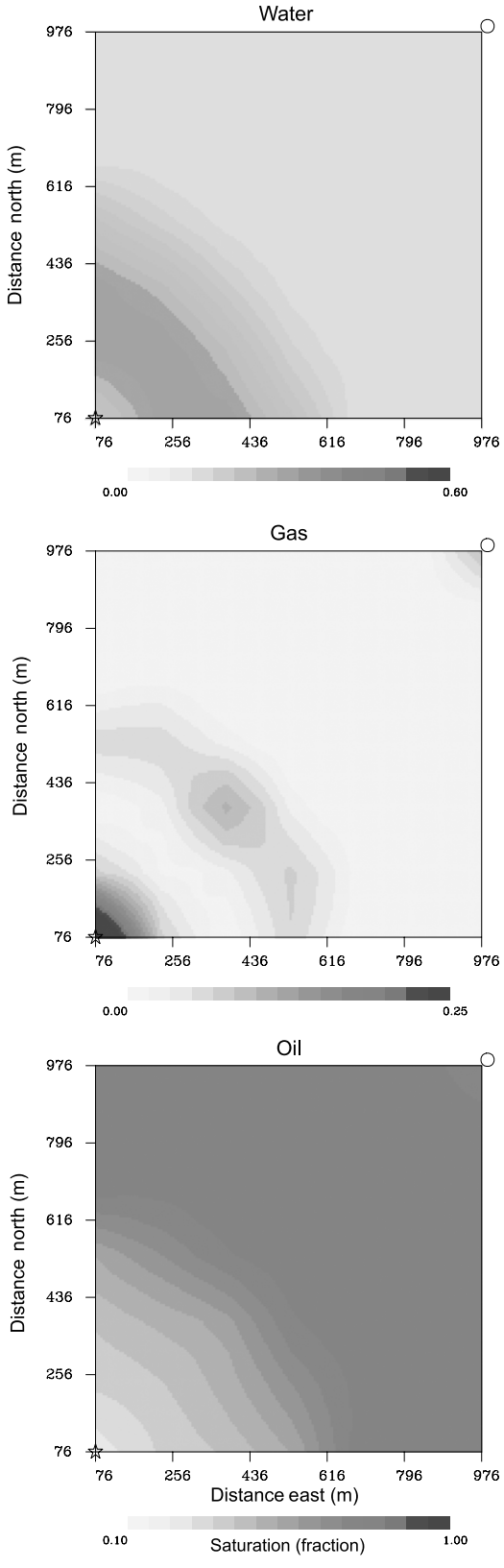

Figure 15. Fluid saturations for water, S_w (top), gas, S_g (middle), and oil, S_o (bottom) after 1096 days of injection. The saturation variations in the middle layer (2543.6–2552.7 m) of the three-layer model are shown.

DISCUSSION

Starting from a fairly general set of governing equations for coupled deformation and flow in a porous medium containing three fluid phases, one can derive expressions for the phase velocities of the various modes of displacement. The expressions are valid in the presence of smoothly varying properties. Because the equations are formulated in the frequency domain, the coefficients of the equations, and hence the expressions for velocity may be functions of frequency. The expressions for the velocities can be used for ray-based modeling of the seismic wavefield (Chapman, 2004). The expressions could also be incorporated into a finite-difference scheme for calculating travel times, in the manner of Vidale (1988) or Sethian (1999). In addition, the asymptotic approach can be used to formulate the transport equation and to compute amplitudes (Chapman, 2004).

The approach taken in this paper allows one to make full use of information routinely available to reservoir engineers. That is, the velocity estimates depend upon the porosity, permeability, relative permeability curves, capillary pressure curves, fluid phase densities, fluid phase viscosities, fluid saturations, and fluid bulk moduli. As indicated in the application to the injection of carbon dioxide, the fluid phase properties output by a compositional simulator can be used directly in the calculations. Furthermore, expressions for the fluid bulk moduli can be derived from the equation of state underlying the compositional reservoir simulation. In the application, the Peng-Robinson equation of state (Peng-Robinson, 1977), one of the default models in the Eclipse simulator, was used. The Peng-Robinson equation of state, one variant of the Van der Waals cubic equations of state (Wei and Sadus, 2000) provides general matches to the bulk modulus variations of hydrocarbon components (Maghari and Hosseinzadeh-Shahri, 2003). The Peng-Robinson

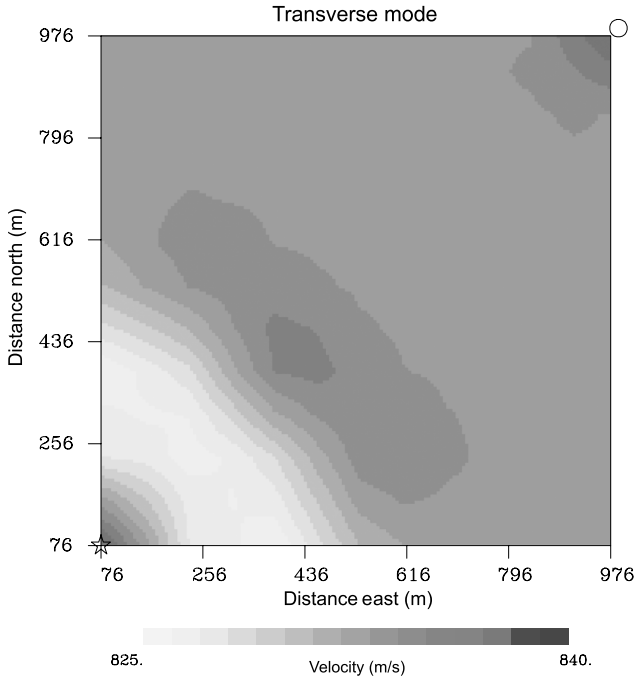

Figure 16. Phase velocity variations associated with the transverse mode of displacement. The velocities in the middle layer (2543.6–2552.7 m) of the three-layer model are shown in this figure.

equation of state has been used extensively to model carbon dioxide injection into reservoirs containing hydrocarbons (Oldenburg et al., 2004; Schlumberger, 2005; Singh et al., 2011).

As noted by Wei and Sadus (2000) many other equations of state are available and there have been many enhancements to the Van der Waals-based equations of state. For example, there are hard-sphere chain equations of state, appropriate for longer chained molecular fluids (Nasrifar and Bolland, 2006). There are equations of state specifically designed for carbon dioxide at a wide range of temperatures and pressures such as that proposed by Span and Wagner (1996) This equation of state appears to give an accurate match to laboratory-derived seismic velocities for temperatures up to 200 K and pressures up to 1000 MPa (Han et al., 2010). Although an equation of state based upon laboratory results is the most accurate, it is difficult to perform experiments under all the possible conditions (pressure, temperature, compositions) encountered during injection and production. For example, the recent experiments of Han et al. (2010) do not consider the effects of changing fluid composition.

For the applications in this paper, I have only accounted for the macroscopic flow, formulated by Biot (1956a, 1956b), as detailed in Appendix A. However, the asymptotic analysis and the expressions for the phase velocity only depend upon the coefficients in the governing equations 15 and 16, and do not require the specific relationship between these coefficients and the rock properties given in Appendix A. In particular, the method can be generalized to include dissipation due to microscopic fluid flow from the pore space to microcracks (Biot, 1962; Mavko and Nur, 1975), often referred to as "squirt-flow." One can also account for intermediate scale or mesoscopic flow, along the lines of a double-porosity model, as was done for a medium containing a single fluid in Pride et al. (2004), or for squirt flow and macroscopic (global) flow using a Zener model (Zener, 1948), as in Carcione and Gurevich (2011). The resulting model is similar to the governing equations presented in this paper. However, the elastic coefficients may now depend upon frequency. Such frequency-dependent coefficients do not present any fundamental difficulty for the approach described in this paper. Because I am working in the frequency domain and the asymptotic expansion is not in terms of frequency, I can apply the same approach to the equations allowing for dissipation due to flow into microcracks.

The approach taken in this paper can be used to extend concepts developed in a single phase context to the situation in which there are multiple phases. For example, by considering the drag forces in the form 5, as in Pride et al. (1993), one can define the transition frequency

$$\omega_0 = \frac{\mu_f \phi}{\rho_f (1+\nu)^{-1} k}, \tag{71}$$

a variation of Biot's characteristic frequency (Biot, 1956). The characteristic frequency separates the low and high frequency domains

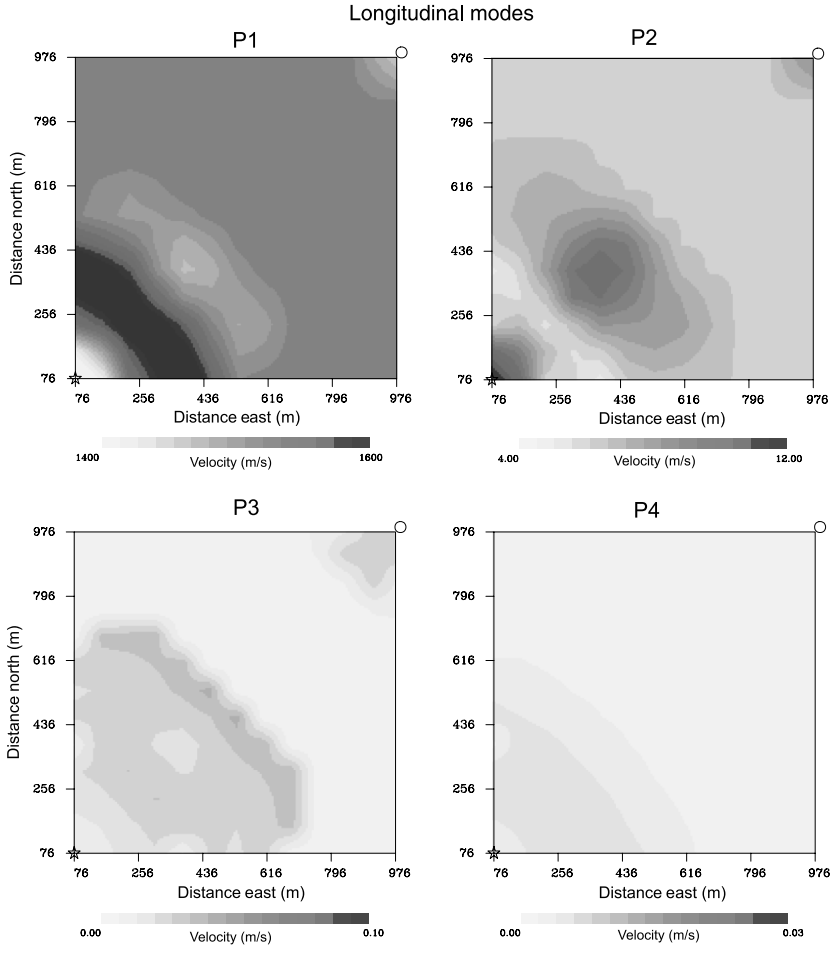

Figure 17. Phase velocity variations associated with the four longitudinal modes of displacement: $P1$, $P2$, $P3$, and $P4$. The velocities in the middle layer (2543.6–2552.7 m) of the three-layer model are shown in this figure.

noted by Biot (1956). In the low-frequency domain, the flow is laminar and the secondary or slow longitudinal modes display a diffusive behavior. In the high-frequency domain, the flow is turbulent and the secondary longitudinal modes begin to exhibit the characteristics of propagating waves. The single phase expression 71 for the characteristic frequency can be generalized to a porous medium containing three fluid phases. To do so, recall the weighted fluid density, introduced in equation 42

$$\rho_f = \chi_1 S_1 \rho_1 + \chi_2 S_2 \rho_2 + \chi_3 S_3 \rho_3 \tag{72}$$

where

$$\chi_i = \frac{\xi_i}{\Gamma_i} = \frac{\nu(1+\nu)^{-1}}{1-\nu(1+\nu)^{-1}}, \tag{73}$$

similarly substitute the weighted fluid viscosity for μ_f

$$\mu_f = \chi_1 S_1 \mu_1 + \chi_2 S_2 \mu_2 + \chi_3 S_3 \mu_3. \tag{74}$$

Thus, in the presence of multiple fluid phases, the transition or characteristic frequency is a function of the properties of the fluids and their saturations. In Figure 18, I plot the characteristic frequency for the three-phase example presented in the Applications section. Note that the characteristic frequency varies between 150 Khz and 350 Khz and is a strong function of the water saturation. This range of values is reasonable and is supported by longitudinal velocity variations in Figure 12, where the velocities of the secondary phases begin to increase significantly at around 100 Khz, signifying a transition in behavior.

One can also reformulate the approach to include the effect of interacting boundaries, extending the approach to laterally varying layered media. That is, one can include the boundary effects in the vertical direction while allowing for lateral variations within a given layer. The interaction of boundaries can have a significant effect on reflections from a thin poroelastic layer (Korneev et al., 2004; Quintal et al., 2011). As in ray-based modeling (Chapman, 2004), one can incorporate boundary conditions into the asymptotic approach and examine the interaction of a propagating disturbance with an interface. For multiple boundaries, one can derive a ray series for various reflections and reverberations (Kennett, 2001).

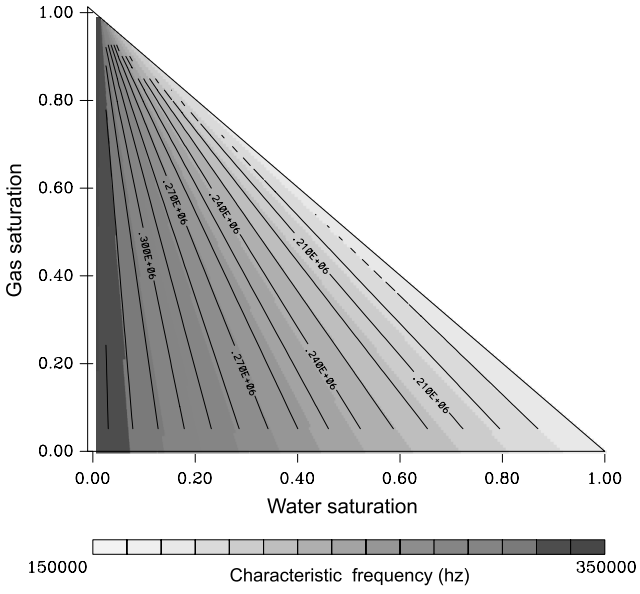

Figure 18. The characteristic frequency, separating the low-frequency laminar flow region in which the secondary longitudinal modes exhibit diffusive behavior from the high-frequency turbulent flow region. In the high-frequency region, the secondary longitudinal modes behave more like propagating waves.

CONCLUSIONS

In this paper, I derive expressions for the phase velocities of the various modes of propagation in a porous medium containing three fluid phases. The approach allows for smoothly varying heterogeneity and fluid saturations, and because I am working in the frequency domain, the velocities may be arbitrary functions of frequency. The motivation for this work is to model the propagation of high-frequency waves through a poroelastic medium containing multiple fluids. The results contained in this paper are a first step in that direction. In future work, I hope to consider amplitudes and the transport equation as well as the reflection and transmission of a propagating disturbance at an interface.

ACKNOWLEDGMENTS

This work was supported by Aramco and by the Assistant Secretary, Office of Basic Energy Sciences of the U. S. Department of Energy under contract DE-AC03-76SF00098. I would also like to acknowledge the support of Aramco. I would like to thank Shingo Watanabe of Texas A&M University for conducting the reservoir simulation for the SPE fifth comparative problem. A Fortran program for the calculation of the velocities associated with the longitudinal modes is available from the author.

APPENDIX A

THE MACROSCOPIC CONSTITUTIVE RELATIONS

In this Appendix, I discuss the stress-strain relationships used in this paper. I begin with the constitutive relations invoked at the microscopic scale. For the solid, I assume linear elastic behavior in which the increment of solid stress, σ_s, is related to the displacement in the solid, $\mathbf{u}_s$, via the expression

$$\sigma_s = K_s \nabla \cdot \mathbf{u}_s \mathbf{I} + G_s \left[\nabla \mathbf{u}_s + (\nabla \mathbf{u}_s)^T - \frac{2}{3} \nabla \cdot \mathbf{u}_s \mathbf{I} \right], \tag{A-1}$$

where K_s is the solid bulk modulus and G_s is the solid shear modulus. The three fluids are taken to be Newtonian in nature. Thus, the fluid stress is related to the flow velocity of the ith fluid phase, $\mathbf{v}_i = \dot{\mathbf{u}}_i$, where the dot indicates the time derivative, according to

$$\sigma_i = -P_i \mathbf{I} + \mu_i \left[\nabla \mathbf{v}_i + (\nabla \mathbf{v}_i)^T - \frac{2}{3} \nabla \cdot \mathbf{v}_i \mathbf{I} \right], \tag{A-2}$$

where P_i is the incremental change in the pore fluid pressure, σ_i is the incremental fluid stress tensor, and μ_i is the shear viscosity.

I can average the constitutive equations A-1 and A-2 over a representative volume V (Bear, 1972, p. 19; Tuncay and Corapcioglu,

1996), making use of a theorem by Slattery (1968, 1981). For the solid component, I have

$$\frac{1}{V}\int_V \sigma_s dV = K_s\left[\nabla\cdot(\alpha_s\bar{\mathbf{u}}_s)+\frac{1}{V}\int_S \mathbf{u}_s\cdot\mathbf{n}dS\right]\mathbf{I} + G_s\left[\nabla(\alpha_s\bar{\mathbf{u}}_s)+\nabla(\alpha_s\bar{\mathbf{u}}_s)^T-\frac{2}{3}\nabla\cdot(\alpha_s\bar{\mathbf{u}}_s)\mathbf{I}+\sum_{i=1}^{3}K_{si}\right], \tag{A-3}$$

where

$$K_{si}=\frac{1}{V}\int_S\left[\mathbf{u}_s\mathbf{n}+\mathbf{n}\mathbf{u}_s-\frac{2}{3}\mathbf{u}_s\cdot\mathbf{n}\mathbf{I}\right]dS \tag{A-4}$$

is a second-order tensor with zero trace (Tuncay and Corapcioglu, 1996). Terms such as $\mathbf{u}_s\mathbf{n}$ are vector outer products that may be thought of as a matrix formed by multiplying the column vector $\mathbf{u}_s$ by the row vector $\mathbf{u}$. If there is no mass change between the solid and liquid phases,

$$\frac{1}{V}\int_S \mathbf{u}_s\cdot\mathbf{n}dS=\alpha_s-\alpha_s^o=\Delta\alpha_s, \tag{A-5}$$

where $\Delta\alpha_s$ is the change in the fraction of the solid phase. Because the displacements are assumed to be small

$$\bar{\mathbf{u}}_j\cdot\nabla\alpha_j\approx 0 \tag{A-6}$$

for $j=s$, 1, 2, 3, and equation A-3 becomes

$$\alpha_s\bar{\sigma}_s = K_s[\alpha_s\nabla\cdot\bar{\mathbf{u}}_s+\Delta\alpha_s]\mathbf{I} + G_s\left[\alpha_s\nabla\bar{\mathbf{u}}_s+\alpha_s(\nabla\bar{\mathbf{u}}_s)^T-\frac{2}{3}\alpha_s\nabla\cdot\bar{\mathbf{u}}_s\mathbf{I}+\sum_{i=1}^{3}K_{si}\right], \tag{A-7}$$

where $\bar{\sigma}_s$ is the intrinsic averaged incremental stress tensor. For the three fluid phases, I have the averaged expressions

$$\alpha_i\bar{\sigma}_i = K_i[\alpha_i\nabla\cdot\bar{\mathbf{u}}_i+\Delta\alpha_i]\mathbf{I} + \mu_i\left[\alpha_i\nabla\bar{\mathbf{v}}_i+\alpha_i(\nabla\bar{\mathbf{v}}_i)^T-\frac{2}{3}\alpha_i\nabla\cdot\bar{\mathbf{v}}_i\mathbf{I}+J_{is}+\sum_{j=1}^{3}J_{ij}\right], \tag{A-8}$$

where

$$J_{ij}=\frac{1}{V}\int_S\left[\mathbf{v}_i\mathbf{n}+\mathbf{n}\mathbf{v}_i-\frac{2}{3}\mathbf{v}_i\cdot\mathbf{n}\mathbf{I}\right]dS \tag{A-9}$$

is a second-order tensor with zero trace (Tuncay and Corapcioglu, 1996).

To fully specify the constitutive equations, I need to determine $\Delta\alpha_s$, and the coupling terms K_{si}, J_{is}, and J_{ij} in equations A-7 and A-8. Given a sufficient number of constraint equations, I can derive an expression for $\Delta\alpha_s$ in terms of the divergences of the solid and fluid displacements. In the next few paragraphs, I assemble the necessary set of equations so that I may determine $\Delta\alpha_s$ as well as K_{si}, J_{is}, and J_{ij}.

First, I invoke the concept of capillary pressure from the physics of fluid flow (Bear, 1972, p. 453; de Marsily, 1986, p. 210). Capillary pressure is the difference in pressure between the various fluids within the averaging volume. That is, there is a jump in pressure at the fluid-fluid interfaces due to interfacial tension that is assumed to depend upon the fluid saturations

$$\bar{P}_1-\bar{P}_2=P_{c12}(S_1,S_2,S_3) \tag{A-10}$$

$$\bar{P}_3-\bar{P}_1=P_{c31}(S_1,S_2,S_3), \tag{A-11}$$

where P_{c12} and P_{c31} are specified functions, typically determined from laboratory experiments on cores and/or fits to proposed functional forms (Wyckoff and Botset, 1936; Van Genuchten, 1980). Note that the capillary pressure functions really only depend upon two of the three fluid saturations because the saturations sum to unity, see equation 1. Because the fluid pressure and saturation changes are incremental and assumed to be small over any small time interval, I can linearize the capillary pressure relationships

$$\bar{P}_1-\bar{P}_2=\frac{\partial P_{c12}}{\partial S_1}\Delta S_1+\frac{\partial P_{c12}}{\partial S_2}\Delta S_2 \tag{A-12}$$

$$\bar{P}_3-\bar{P}_1=\frac{\partial P_{c31}}{\partial S_1}\Delta S_1+\frac{\partial P_{c31}}{\partial S_2}\Delta S_2. \tag{A-13}$$

To complete the specification of the constitutive relation between the stresses and the displacements, I subdivide the material that follows into two subsections. The first subsection treats the isotropic component of the stresses and the divergence of the displacement vector fields. The shear modulus of the solid frame enters the constitutive equation in the final subsection when I consider the deviatoric component of the displacement due to a shear stress. Because I have chosen to represent viscous forces as the coupling terms $\mathbf{d}_j$ in equations 3 and 4, the effects of permeability and relative permeabilities will enter later, through the dynamic tortuosity.

Volumetric component

By considering the volumetric component of the constitutive equations, I can relate the solid and fluid pressures to the divergence of the respective displacements. In fact, I define the solid and fluid pressures in terms of the trace of the averaged incremental stress tensor

$$\alpha_j\bar{P}_j=-\frac{1}{3}\,tr(\alpha_j\bar{\sigma}_j)=-K_j(\alpha_j\nabla\cdot\bar{\mathbf{u}}_j+\Delta\alpha_j) \tag{A-14}$$

for $j=s$, 1, 2, 3. In writing equation A-14, I have made use of equations A-7 and A-8 and the fact that the trace of the factors K_{si}, J_{is}, and J_{ij} vanish. I can rearrange equation A-14 and write it as a relationship between $\Delta\alpha_j$, $\bar{P}_j$, and $\nabla\cdot\bar{\mathbf{u}}_j$,

$$K_j\Delta\alpha_j+\alpha_j\bar{P}_j=-K_j\alpha_j\nabla\cdot\bar{\mathbf{u}}_j. \tag{A-15}$$

Equation A-15 may be written solely in terms of the change in the solid volume fraction ($\Delta\alpha_s$) and the fluid saturation changes (ΔS_1 and ΔS_2) if I use the fact that

$$\alpha_i = S_i\phi = S_i(1-\alpha_s) \tag{A-16}$$

[see equation 2]. Because ΔS_j and $\Delta\alpha_s$ are assumed to be small, I can use equation A-16 to write

$$\Delta\alpha_i = \Delta[S_i(1-\alpha_s)] \approx (1-\alpha_s)\Delta S_i - S_i\Delta\alpha_s. \tag{A-17}$$

Thus, I can write equation A-15 in terms of $\Delta\alpha_s$, ΔS_j, and $\bar{P}_j$

$$-S_jK_j\Delta\alpha_s + \phi K_j\Delta S_j + \alpha_j\bar{P}_j = -K_j\alpha_j\nabla\cdot\bar{\mathbf{u}}_j. \tag{A-18}$$

Note that, because the saturations sum to unity, I can write the expression for $\Delta\alpha_3$ entirely in terms of ΔS_1, ΔS_2, and $\Delta\alpha_s$. To keep the equations simpler, I retain S_3 in many of the formulas presented below. When necessary S_3 may be replaced by $S_3 = 1 - S_1 - S_2$ if I wish to eliminate it from the equations.

An additional constraint is provided by a generalization of the single phase relationship derived by Pride et al. (1992) which relates the divergence of the solid displacement field to the fluid and solid pressures

$$\nabla\cdot\bar{\mathbf{u}}_s = -\alpha_s\frac{(\bar{P}_s-\bar{P}_f)}{K_{fr}} - \frac{\bar{P}_f}{K_s}. \tag{A-19}$$

Following Tuncay and Corapcioglu (1996) I write the fluid pressure as a weighted sum of the phase pressures, where the weights are the fluid saturations

$$\bar{P}_f = \sum_{i=1}^{3} S_i\bar{P}_i. \tag{A-20}$$

Upon substituting A-20 into equation A-19 and rearranging terms I have the final constraint

$$-\frac{1}{K_w}\bar{P}_s + D_k\sum_{i=1}^{3} S_i\bar{P}_i = \nabla\cdot\bar{\mathbf{u}}_s, \tag{A-21}$$

where

$$K_w = \frac{K_{fr}}{\alpha_s} \tag{A-22}$$

and

$$D_k = \frac{\alpha_s}{K_{fr}} - \frac{1}{K_s}. \tag{A-23}$$

Equations A-10, A-11, A-15 or its alternative version A-18, and A-21 constitute a system of seven equations in the seven unknowns $\Delta\alpha_s$, ΔS_1, ΔS_2, $\bar{P}_s$, $\bar{P}_1$, $\bar{P}_2$, and $\bar{P}_3$. I may write the linear system of equations in matrix-vector form

$$\mathbf{K}\Delta = \Upsilon, \tag{A-24}$$

where $\mathbf{K}$ is the coefficient matrix

$$\begin{pmatrix} 0 & P_{c12,1} & P_{c12,2} & 0 & -1 & 1 & 0 \\ 0 & P_{c31,1} & P_{c31,2} & 0 & 1 & 0 & -1 \\ 1 & 0 & 0 & \frac{\alpha_s}{K_s} & 0 & 0 & 0 \\ -S_1 & \phi & 0 & 0 & \frac{\alpha_1}{K_1} & 0 & 0 \\ -S_2 & 0 & \phi & 0 & 0 & \frac{\alpha_2}{K_2} & 0 \\ -S_3 & -\phi & -\phi & 0 & 0 & 0 & \frac{\alpha_3}{K_3} \\ 0 & 0 & 0 & -{K_w}^{-1} & S_1D_k & S_2D_k & S_3D_k \end{pmatrix}, \tag{A-25}$$

$$\Delta = \begin{pmatrix} \Delta\alpha_s \\ \Delta S_1 \\ \Delta S_2 \\ \bar{P}_s \\ \bar{P}_1 \\ \bar{P}_2 \\ \bar{P}_3 \end{pmatrix} \tag{A-26}$$

and

$$\Upsilon = \begin{pmatrix} 0 \\ 0 \\ -\alpha_s\nabla\cdot\bar{\mathbf{u}}_s \\ -\alpha_1\nabla\cdot\bar{\mathbf{u}}_1 \\ -\alpha_2\nabla\cdot\bar{\mathbf{u}}_2 \\ -\alpha_3\nabla\cdot\bar{\mathbf{u}}_3 \\ \nabla\cdot\bar{\mathbf{u}}_s \end{pmatrix}, \tag{A-27}$$

where

$$P_{c12,j} = \frac{\partial P_{c12}}{\partial S_j}, \tag{A-28}$$

and

$$P_{c31,j} = \frac{\partial P_{c31}}{\partial S_j}. \tag{A-29}$$

Because the system of equations A-24 is linear, I can solve for the unknowns as linear functions of the right side.

At this juncture, I can follow one of two possible paths. On the one hand, if I were primarily interested in computing velocities and do not require explicit expressions in terms of the fundamental material constants in the matrix $\mathbf{K}$, I could invert the matrix A-25 numerically and solve for the pressures $\bar{P}_s$, $\bar{P}_1$, $\bar{P}_2$, and $\bar{P}_3$ in terms of the divergences on the right side of equation A-24. On the other hand, if I desire explicit expressions for the coefficients of the constitutive relationship in terms of the fundamental quantities, then I must construct an analytic expression for the solution of equation A-24. One difficulty with this second approach is that the coefficient matrix A-25 is 7×7 and, even though the matrix is sparse, solving for all seven unknowns will produce a rather involved expression. I can reduce the complexity of the analytic expressions somewhat, reducing the sparse coefficient matrix A-25 to a dense

3×3 matrix, by first eliminating the variables $\Delta\alpha_s$, ΔS_1, ΔS_2, and $\bar{P}_3$. However, the final analytic expressions are still rather involved and thus more prone to result in errors in their specification and in their numerical implementation.

Consider the first approach, in which I solve the system of equations A-24 numerically. Let us denote the inverse of the coefficient matrix $\mathbf{K}$ by matrix $\mathbf{B}$ with elements B_{ij}. Because of the structure of the right side of equations A-24, given by the vector Υ (expression A-27), I can write the expression for $\bar{P}_s$ as

$$\alpha_s \bar{P}_s = a_{ss} \nabla \cdot \bar{\mathbf{u}}_s + \sum_{j=1}^{3} a_{sj} \nabla \cdot \bar{\mathbf{u}}_j \tag{A-30}$$

where

$$a_{ss} = \alpha_s (B_{47} - B_{43} \alpha_s) \tag{A-31}$$

$$a_{sj} = -\alpha_s \alpha_j B_{4(j+3)}. \tag{A-32}$$

And similarly, for the ith fluid phase I have the expressions

$$\alpha_i \bar{P}_i = a_{is} \nabla \cdot \bar{\mathbf{u}}_s + \sum_{j=1}^{3} a_{ij} \nabla \cdot \bar{\mathbf{u}}_j \tag{A-33}$$

where the coefficients are given by

$$a_{is} = \alpha_i (B_{(4+i)7} - B_{(4+i)3} \alpha_s) \tag{A-34}$$

$$a_{ij} = -\alpha_i \alpha_j B_{(4+i)(j+3)}. \tag{A-35}$$

Deviatoric component

To complete the specification of the constitutive relations, I consider the deviatoric component due to the application of an external shear stress. As in Tuncay and Corapcioglu (1996), I assume that all shear resistance of the porous medium is due to the solid matrix and that the fluid does not contribute. Thus, the shear deformation of fluid phases is uncoupled and $K_{si} = J_{is} = J_{ij}$. Essentially, I am assuming that, for the sake of the constitutive relationship, the fluid viscosities are negligible in equation A-8 in comparison with the volumetric component and the bulk modulus. The effect of fluid viscosities, present in the momentum equation, will be included as momentum transfer vectors between phases, $\mathbf{d}_j$, as discussed in the main body of the paper [see equations 3 and 4]. Thus, the deviatoric component of $\bar{\sigma}_s$, denoted by $\bar{\sigma}_s^D$, is given by

$$\alpha_s \bar{\sigma}_s^D = G_{fr} \left[\nabla \bar{\mathbf{u}}_s + (\nabla \bar{\mathbf{u}}_s)^T - \frac{2}{3} \nabla \cdot \bar{\mathbf{u}}_s \mathbf{I} \right], \tag{A-36}$$

where G_{fr} is the frame shear modulus, typically determined from experiments on the unsaturated sample.

The complete constitutive relationship

Putting everything together, I have the following constitutive relationships

$$\alpha_s \bar{\sigma}_s = \left[a_{ss} \nabla \cdot \bar{\mathbf{u}}_s + \sum_{j=1}^{3} a_{sj} \nabla \cdot \mathbf{u}_j \right] \mathbf{I} + G_{fr} \left[\nabla \bar{\mathbf{u}}_s + (\nabla \bar{\mathbf{u}}_s)^T - \frac{2}{3} \nabla \cdot \bar{\mathbf{u}}_s \mathbf{I} \right] \tag{A-37}$$

and

$$\alpha_i \bar{\sigma}_i = \left[a_{is} \nabla \cdot \bar{\mathbf{u}}_i + \sum_{j=1}^{3} a_{ij} \nabla \cdot \bar{\mathbf{u}}_j \right] \mathbf{I} \tag{A-38}$$

for the solid and fluid phases, respectively.

The constitutive relationship in terms of $\bar{\mathbf{u}}_s$ and $\bar{\mathbf{w}}_s$

Because the final formulation will be in terms of $\bar{\mathbf{u}}_s$ and $\bar{\mathbf{w}}_i$ where $\bar{\mathbf{w}}_i = \bar{\mathbf{u}}_i - \bar{\mathbf{u}}_s$, I need to convert to those variables. I can rewrite the constitutive relationships in terms of the new variables by adding and subtracting $\bar{\mathbf{u}}_s$. The result is

$$\alpha_s \bar{\sigma}_s = \left[\hat{a}_{ss} \nabla \cdot \bar{\mathbf{u}}_s + \sum_{i=1}^{3} a_{si} \nabla \cdot \mathbf{w}_i \right] \mathbf{I} + G_{fr} \left[\nabla \bar{\mathbf{u}}_s + (\nabla \bar{\mathbf{u}}_s)^T - \frac{2}{3} \nabla \cdot \bar{\mathbf{u}}_s \mathbf{I} \right] \tag{A-39}$$

and

$$\alpha_i \bar{\sigma}_i = \left[\hat{a}_{is} \nabla \cdot \bar{\mathbf{u}}_s + \sum_{j=1}^{3} a_{ij} \nabla \cdot \mathbf{w}_j \right] \mathbf{I} \tag{A-40}$$

for the solid and fluid phases, respectively, with the adjusted coefficients of $\nabla \cdot \bar{\mathbf{u}}_s$

$$\hat{a}_{ss} = a_{ss} + a_{s1} + a_{s2} + a_{s3} \tag{A-41}$$

$$\hat{a}_{is} = a_{is} + a_{i1} + a_{i2} + a_{i3} \tag{A-42}$$

for $i = 1, 2, 3$. Finally, I can rename the coefficients so that they follow the notation of Vasco and Minkoff (2012) for two-phase flow. This notation is intended to maintain continuity with developments in single-phase flow (Pride, 2005; Vasco, 2009). Thus, I define the variables found in the governing equations 15 and 16

$$K_u = \hat{a}_{ss}, \tag{A-43}$$

$$C_{si} = a_{is}, \tag{A-44}$$

$$C_{is} = \hat{a}_{is}, \tag{A-45}$$

$$M_{ij} = a_{ij}, \tag{A-46}$$

and

$$G_m = G_{fr}. \tag{A-47}$$

APPENDIX B

COMPUTING THE DETERMINANT ASSOCIATED WITH THE LONGITUDINAL MODES

In this Appendix, I present the expressions for the coefficients of the quartic equation 50 that determines $s = l^2$, where l is the magnitude of the vector $\mathbf{l} = \nabla\theta$. The approach for calculating the coefficients is described in Vasco and Minkoff (2012). The essential idea relates to the expansion of the determinant of the matrix

$$\mathbf{M} = \begin{pmatrix} \nu_s - Hs & \xi_1 - C_{s1}s & \xi_2 - C_{s2}s & \xi_3 - C_{s3}s \\ \nu_1 - C_{1s}s & \Gamma_1 - M_{11}s & -M_{12}s & -M_{13}s \\ \nu_2 - C_{2s}s & -M_{21}s & \Gamma_2 - M_{22}s & -M_{23}s \\ \nu_3 - C_{3s}s & -M_{31}s & -M_{32}s & \Gamma_3 - M_{33}s \end{pmatrix}. \tag{B-1}$$

The determinant of $\mathbf{M}$ can be expanded using the formula for the determinant of a matrix in which a column is the sum of two components (Noble and Daniel, 1977, p. 200), as noted in the main body of the text (see equation 49). I can apply this rule recursively because every column of $\mathbf{M}$ may be described as such a sum. Thus, I can write the equation

$$\det \mathbf{M} = 0 \tag{B-2}$$

as the quartic equation

$$Q_4 s^4 - Q_3 s^3 + Q_2 s^2 - Q_1 s + Q_0 = 0, \tag{B-3}$$

with the coefficients

$$Q_4 = \begin{vmatrix} H & C_{s1} & C_{s2} & C_{s_3} \\ C_{1s} & M_{11} & M_{12} & M_{13} \\ C_{2s} & M_{21} & M_{22} & M_{23} \\ C_{3s} & M_{31} & M_{32} & M_{33} \end{vmatrix}, \tag{B-4}$$

$$Q_3 = \begin{vmatrix} \nu_s & C_{s1} & C_{s2} & C_{s_3} \\ \nu_1 & M_{11} & M_{12} & M_{13} \\ \nu_2 & M_{21} & M_{22} & M_{23} \\ \nu_3 & M_{31} & M_{32} & M_{33} \end{vmatrix} + \begin{vmatrix} H & \xi_1 & C_{s2} & C_{s_3} \\ C_{1s} & \Gamma_1 & M_{12} & M_{13} \\ C_{2s} & 0 & M_{22} & M_{23} \\ C_{3s} & 0 & M_{32} & M_{33} \end{vmatrix} + \begin{vmatrix} H & C_{s1} & \xi_2 & C_{s_3} \\ C_{1s} & M_{11} & 0 & M_{13} \\ C_{2s} & M_{21} & \Gamma_2 & M_{23} \\ C_{3s} & M_{31} & 0 & M_{33} \end{vmatrix} + \begin{vmatrix} H & C_{s1} & C_{s2} & \xi_3 \\ C_{1s} & M_{11} & M_{12} & 0 \\ C_{2s} & M_{21} & M_{22} & 0 \\ C_{3s} & M_{31} & M_{32} & \Gamma_3 \end{vmatrix}, \tag{B-5}$$

$$Q_2 = \begin{vmatrix} \nu_s & \xi_1 & C_{s2} & C_{s_3} \\ \nu_1 & \Gamma_1 & M_{12} & M_{13} \\ \nu_2 & 0 & M_{22} & M_{23} \\ \nu_3 & 0 & M_{32} & M_{33} \end{vmatrix} + \begin{vmatrix} \nu_s & C_{s1} & \xi_2 & C_{s_3} \\ \nu_1 & M_{11} & 0 & M_{13} \\ \nu_2 & M_{21} & \Gamma_2 & M_{23} \\ \nu_3 & M_{31} & 0 & M_{33} \end{vmatrix} + \begin{vmatrix} \nu_s & C_{s1} & C_{s2} & \xi_3 \\ \nu_1 & M_{11} & M_{12} & 0 \\ \nu_2 & M_{21} & M_{22} & 0 \\ \nu_3 & M_{31} & M_{32} & \Gamma_3 \end{vmatrix} + \begin{vmatrix} H & \xi_1 & \xi_2 & C_{s_3} \\ C_{1s} & \Gamma_1 & 0 & M_{13} \\ C_{2s} & 0 & \Gamma_2 & M_{23} \\ C_{3s} & 0 & 0 & M_{33} \end{vmatrix}, \tag{B-6}$$

$$Q_1 = \begin{vmatrix} \nu_s & \xi_1 & \xi_2 & C_{s_3} \\ \nu_1 & \Gamma_1 & 0 & M_{13} \\ \nu_2 & 0 & \Gamma_2 & M_{23} \\ \nu_3 & 0 & 0 & M_{33} \end{vmatrix} + \begin{vmatrix} \nu_s & \xi_1 & C_{s2} & \xi_3 \\ \nu_1 & \Gamma_1 & M_{12} & 0 \\ \nu_2 & 0 & M_{22} & 0 \\ \nu_3 & 0 & M_{32} & \Gamma_3 \end{vmatrix} + \begin{vmatrix} \nu_s & C_{s1} & \xi_2 & \xi_3 \\ \nu_1 & M_{11} & 0 & 0 \\ \nu_2 & M_{21} & \Gamma_2 & 0 \\ \nu_3 & M_{31} & 0 & \Gamma_3 \end{vmatrix} + \begin{vmatrix} H & \xi_1 & \xi_2 & \xi_3 \\ C_{1s} & \Gamma_1 & 0 & 0 \\ C_{2s} & 0 & \Gamma_2 & 0 \\ C_{3s} & 0 & 0 & \Gamma_3 \end{vmatrix}, \tag{B-7}$$

and

$$Q_0 = \begin{vmatrix} \nu_s & \xi_1 & \xi_2 & \xi_3 \\ \nu_1 & \Gamma_1 & 0 & 0 \\ \nu_2 & 0 & \Gamma_2 & 0 \\ \nu_3 & 0 & 0 & \Gamma_3 \end{vmatrix}, \tag{B-8}$$

where the vertical bars signify that the quantity is the determinant of the enclosed matrix.

REFERENCES

Aki, K., and P. G. Richards, 1980, Quantitative seismology: Freeman and Sons.

Anile, A. M., J. K. Hunter, P. Pantano, and G. Russo, 1993, Ray methods for nonlinear waves in fluids and plasmas: Longman Scientific and Technical.

Arts, R., O. Eiken, R. A. Chadwick, P. Zweigel, L. van der Meer, and B. Zinszner, 2004, Monitoring of CO_2 injected at Sleipner using time-lapse seismic data: Energy, **29**, 1383–1392, doi: 10.1016/j.energy.2004.03.072.

Aziz, K., and A. Settari, 1979, Petroleum reservoir simulation: Applied Science Publishers.

Baker, L. E., 1988, Three-phase relative permeability correlations, proceedings of the SPE/DOE symposium on enhanced oil recovery: SPE paper 17369, 17–20.

Batzle, M., R. Christiansen, and D.-H. Han, 1998, Reservoir recovery processes and geophysics: The Leading Edge, **17**, 1444–1447, doi: 10.1190/1.1437872.

Batzle, M., and Z. Wang, 1992, Seismic properties of pore fluids: Geophysics, **57**, 1396–1408, doi: 10.1190/1.1443207.

Bear, J., 1972, Dynamics of fluids in porous media: Elsevier.

Ben-Menahem, A., and S. J. Singh, 1981, Seismic waves and sources: Springer Verlag.

Berryman, J. G., L. Thigpen, and R. C. Y. Chin, 1988, Bulk elastic wave propagation in partially saturated porous solids: Journal of the Acoustical Society of America, **84**, 360–373, doi: 10.1121/1.396938.

Biot, M. A., 1956a, Theory of propagation of elastic waves in a fluid-saturated porous solid. Part I: Low frequency range: Journal of the Acoustical Society of America, **28**, 168–178, doi: 10.1121/1.1908239.

Biot, M. A., 1956b, Theory of propagation of elastic waves in a fluid-saturated porous solid. Part I: Higher frequency range: Journal of the Acoustical Society of America, **28**, 179–191, doi: 10.1121/1.1908241.

Biot, M. A., 1962a, Mechanics of deformation and acoustic propagation in porous media: Journal of Applied Physics, **33**, 1482–1498, doi: 10.1063/1.1728759.

Biot, M. A., 1962b, Generalized theory of acoustic propagation in porous dissipative media: Journal of the Acoustical Society of America, **34**, 1254–1264, doi: 10.1121/1.1918315.

Blunt, M. J., 2000, An empirical model for three-phase relative permeability: SPE Journal, **5**, 435–445, doi: 10.2118/67950-PA.

Carcione, J. M., and B. Gurevich, 2011, Differential form and numerical implementation of Biot's poroelasticity equations with squirt dissipation: Geophysics, **76**, no. 6, N55–N64, doi: 10.1190/geo2010-0169.1.

Carcione, J. M., S. Picotti, D. Gei, and G. Rossi, 2006, Physics and seismic modeling for monitoring CO_2 storage: Pure and Applied Geophysics, **163**, 175–207, doi: 10.1007/s00024-005-0002-1.

Chapman, C. H., 2004, Fundamentals of seismic wave propagation: Cambridge University Press.

Clark, A., 1984, Elements of abstract algebra: Dover Publications Incorporated.

Corey, A. T., C. H. Rathjens, J. H. Henderson, and M. R. J. Wyllie, 1956, Three-phase relative permeability: Transactions of the Society of Petroleum Engineers of the American Institute of Mining, Metallurgical, and Petroleum Engineers, Inc, **207**, 349–351.

Courant, R., and D. Hilbert, 1962, Methods of mathematical physics: Interscience.

de Marsily, G., 1986, Quantitative hydrogeology: Academic Press.

Dvorkin, J., R. Nolen-Hoeksema, and A. Nur, 1994, The squirt-flow mechanism: Macroscopic description: Geophysics, **59**, 428–438, doi: 10.1190/1.1443605.

Faucette, W. J., 1996, A geometric interpretation of the solution of the general quartic polynomial: American Mathematical Monthly, **103**, 51–57, doi: 10.2307/2975214.

Friedlander, F. G., and J. B. Keller, 1955, Asymptotic expansions of solutions of $(\nabla^2 + k^2)u = 0$: Communications on Pure and Applied Mathematics, **8**, 387–394, doi: 10.1002/(ISSN)1097-0312.

Garg, S. K., 1971, Wave propagation in a fluid-saturated porous solid: Journal of Geophysical Research, **76**, 7947–7962, doi: 10.1029/JB076i032p07947.

Gassmann, F., 1951, Elastic waves through a packing of spheres: Geophysics, **16**, 673–685, doi: 10.1190/1.1437718.

Han, D-H., M. Sun, and M. Batzle, 2010, CO_2 velocity measurements and models for temperatures up to 200° and pressures up to 100 mpa: Geophysics, **75**, no. 3, E123–E129, doi: 10.1190/1.3383324.

Hoversten, G. M., R. Gritto, J. Washbourne, and T. Daley, 2003, Pressure and fluid saturation prediction in a multicomponent reservoir using combined seismic and electromagnetic imaging: Geophysics, **68**, 1580–1591, doi: 10.1190/1.1620632.

JafarGandomi, A., and A. Curtis, 2011, Detectability of petrophysical properties of subsurface CO_2-saturated aquifer reservoirs using surface geophysical methods: The Leading Edge, **30**, 1112–1121, doi: 10.1190/1.3657069.

Jerauld, G. R., 1997, General three-phase relative permeability model for Prudhoe bay: SPE Reservoir Engineering, **12**, 255–263.

Johnson, D. L., 1987, Theory of dynamic permeability and tortuosity in fluid-saturated porous media: Journal of Fluid Mechanics, **176**, 379–402, doi: 10.1017/S0022112087000727.

Jones, T. D., 1986, Pore fluids and frequency-dependent wave propagation in rocks: Geophysics, **51**, 1939–1953, doi: 10.1190/1.1442050.

Kazemeini, S. H., C. Juhlin, and S. Fomel, 2010, Monitoring CO_2 response on surface seismic data; a rock physics and seismic modeling feasibility study at the CO_2 sequestration site, Ketzin, Germany: Journal of Applied Geophysics, **71**, 109–124, doi: 10.1016/j.jappgeo.2010.05.004.

Kennett, B. L. N., 2001, The seismic wavefield: Cambridge University Press.

Killough, J., and C. Kossack, 1987, Fifth SPE comparative solution project: Evaluation of miscible flood simulators: SPE Reservoir Engineering, Paper 16000: 1987 SPE Reservoir Simulation Symposium.

Kline, M., and I. W. Kay, 1965, Electromagnetic theory and geometrical optics: John Wiley and Sons.

Korneev, V. A., G. M. Goloshubin, T. M. Daley, and D. B. Silin, 2004, Seismic low-frequency effects in monitoring fluid-saturated reservoirs: Geophysics, **69**, 522–532, doi: 10.1190/1.1707072.

Leverett, M. C., and W. B. Lewis, 1941, Steady flow of gas-oil-water mixtures through unconsolidated sands: Transactions of the Society of Petroleum Engineers of the American Institute of Mining, Metallurgical, and Petroleum Engineers, Inc, **142**, 107–116.

Lo, W.-C., G. Sposito, and E. Majer, 2005, Wave propagation through elastic porous media containing two immiscible fluids: Water Resources Research, **41**, 1–20, doi: 10.1029/2004WR003162.

Lo, W.-C., G. Sposito, and E. Majer, 2009, Analytical decoupling of poroelasticity equations for acoustic-wave propagation and attenuation in a porous medium containing two immiscible fluids: Journal of Engineering Mathematics, **64**, 219–235, doi: 10.1007/s10665-008-9254-y.

Luneburg, R. K., 1966, Mathematical theory of optics: University of California Press.

Maghari, A., and L. Hosseinzadeh-Shahri, 2003, Evaluation of the performance of cubic equations of state in predicting regularities in dense fluids: Fluid Phase Equilibria, **206**, 287–311, doi: 10.1016/S0378-3812(03)00008-6.

Mavko, G., and A. Nur, 1975, Melt squirt in the aesthenosphere: Journal of Geophysical Research, **80**, 1444–1448, doi: 10.1029/JB080i011p01444.

Menke, W., 1989, Geophysical data analysis: Discrete inverse theory: Academic Press.

Mualem, Y., 1976, A new model for predicting the hydraulic conductivity of unsaturated porous media: Water Resources Research, **12**, 513–522, doi: 10.1029/WR012i003p00513.

Nasrifar, K., and O. Bolland, 2006, Simplified hard-sphere and hard-sphere chain equations of state for engineering applications: Chemical Engineering Communications, **193**, 1277–1293, doi: 10.1080/00986440500511262.

Nickalls, R. W. D., 2009, The quartic equation: Invariants and Euler's solution revealed: The Mathematical Gazette, **93**, 66–75.

Noble, B., and J. W. Daniel, 1977, Applied linear algebra: Prentice-Hall.

O'Connell, R. J., and B. Budiansky, 1977, Viscoelastic properties of fluid-saturated cracked solids: Journal of Geophysical Research, **82**, 5719–5735, doi: 10.1029/JB082i036p05719.

Oldenburg, C. M., G. J. Moridis, N. Spycher, and K. Pruess, 2004, Eos7c version 1.0: Tough2 module for carbon dioxide or nitrogen in natural gas (methane) reservoirs: LBNL Report, 56589, 1–53.

Parker, J. C., R. J. Lenhard, and T. Kuppusamy, 1987, A parametric model of constitutive properties governing multiphase flow in porous media: Water Resources Research, **23**, 618–624, doi: 10.1029/WR023i004p00618.

Peaceman, D. W., 1977, Fundamentals of numerical reservoir simulation: Elsevier Scientific Publishing Company.

Peng, D. Y., and D. B. Robinson, 1977, A rigorous method for predicting the critical properties of multicomponent systems from an equation of state: AIChE Journal, **23**, 137–144, doi: 10.1002/(ISSN)1547-5905.

Pham, N. H., J. M. Carcione, H. B. Helle, and B. Ursin, 2002, Wave velocities and attenuation of shaley sandstones as a function of pore pressure and partial saturation: Geophysical Prospecting, **50**, 615–627, doi: 10.1046/j.1365-2478.2002.00343.x.

Pride, S. R., 2005, Relationships between seismic and hydrological properties: Hydrogeophysics: Springer, 253–291.

Pride, S. R., J. G. Berryman, and J. M. Harris, 2004, Seismic attenuation due to wave induced flow: Journal of Geophysical Research, **109**, B01201, doi: 10.1029/2003JB002639.

Pride, S. R., A. F. Gangi, and F. D. Morgan, 1992, Deriving the equations of motion for isotropic motion: Journal of the Acoustical Society of America, **92**, 3278–3290, doi: 10.1121/1.404178.

Pride, S. R., F. D. Morgan, and A. F. Gangi, 1993, Drag forces of porous-medium acoustics: Physical Review B, **47**, 4964–4978, doi: 10.1103/PhysRevB.47.4964.

Quintal, B., S. M. Schmalholz, and Y. Y. Podladchikov, 2011, Impact of fluid saturation on the reflection coefficient of a poroelastic layer: Geophysics, **76**, no. 2, N1–N12, doi: 10.1190/1.3553002.

Santos, J. E., J. M. Corbero, and J. Douglas, 1990, Static and dynamic behavior of a porous solid saturated by a two-phase fluid: Journal of the Acoustical Society of America, **87**, 1428–1438, doi: 10.1121/1.399439.

Sarem, A. M., 1966, Three-phase relative permeability measurements by unsteady-state method: SPE Journal, **6**, 199–205.

Schlumberger, Abingdon Technology Center, 2005, PVTI and Eclipse 3000: An introduction to PVT analysis and compositional simulation: Schlumberger Information Systems, Houston.

Sethian, J. A., 1999, Level set methods: Cambridge University Press.

Shi, J.-Q., Z. Xue, and S. Durucan, 2007, Seismic monitoring and modelling of supercritical CO_2 injection into a water-saturated sandstone: Interpretation of P-wave velocity data: International Journal of Greenhouse Gas Control, **1**, 473–480.

Silvester, J. R., 2000, Determinants of block matrices: The Mathematical Gazette, **84**, 460–467.

Singh, A. K., U.-J. Goerke, and O. Kolditz, 2011, Numerical simulation of non-isothermal compositional gas flow: Application to carbon dioxide injection into gas reservoirs: Energy, **36**, 3446–3458, doi: 10.1016/j.energy.2011.03.049.

Slattery, J. C., 1968, Multiphase viscoelastic fluids through porous media: AIChE Journal, **14**, 50–56, doi: 10.1002/(ISSN)1547-5905.

Slattery, J. C., 1981, Momentum, energy, and mass transfer in continua: Krieger.

Smith, T. M., C. H. Sondergeld, and C. S. Rai, 2003, Gassmann fluid substitutions: A tutorial: Geophysics, **68**, 430–440, doi: 10.1190/1.1567211.

Span, R., and W. Wagner, 1996, A new equation of state for carbon dioxide covering the fluid region from the triple-point temperature to 1100 k at pressures up to 800 mpa: Journal of Physical and Chemical Reference Data, **25**, 1509–1596, doi: 10.1063/1.555991.
Spiegel, M. R., 1959, Theory and problems of vector analysis: McGraw-Hill Book Company.
Stahl, S., 1997, Introductory modern algebra: John Wiley and Sons.
Stone, H. L., 1973, Estimation of three-phase relative permeability and residual oil data: Journal of Canadian Petroleum Technology, **12**, 53–61.
Tuncay, K., 1995, Wave propagation in single- and double-porosity deformable porous media saturated by multiphase fluids: Ph.D. dissertation, Texas A&M University.
Tuncay, K., and M. Y. Corapcioglu, 1996, Body waves in poroelastic media saturated by two immiscible fluids: Journal of Geophysical Research, **101**, 25149–25159, doi: 10.1029/96JB02297.
Tuncay, K., and M. Y. Corapcioglu, 1997, Wave propagation in poroelastic media saturated by two fluids: Journal of Applied Mechanics and Technical Physics, **64**, 313–320.
Van Genuchten, M. T., 1980, A closed form equation for predicting the hydraulic conductivity of unsaturated soils: Soil Science Society of America Journal, **44**, 892–898, doi: 10.2136/sssaj1980.03615995004400050002x.
Vasco, D. W., 2009, Modeling broadband poroelastic propagation using an asymptotic approach: Geophysical Journal International, **179**, 299–318, doi: 10.1111/gji.2009.179.issue-1.
Vasco, D. W., H. Keers, J. Peterson, and E. L. Majer, 2003, Zeroth order asymptotics: Waveform inversion of the lowest degree: Geophysics, **68**, 614–628, doi: 10.1190/1.1567231.
Vasco, D. W., and S. E. Minkoff, 2012, On the propagation of a disturbance in a heterogeneous, deformable, porous medium saturated with two fluid phases: Geophysics, **77**, no. 3, L25–L44, doi: 10.1190/geo2011-0131.1.
Vidale, J., 1988, Finite-difference calculation of travel times: Bulletin of the Seismological Society of America, **78**, 2062–2076.
Wei, Y. S., and R. J. Sadus, 2000, Equations of state for the calculation of fluid-phase equilibria: AIChE Journal, **46**, 169–196, doi: 10.1002/(ISSN)1547-5905.
White, J. E., 1975, Computed seismic speeds and attenuation in rocks with partial gas saturation: Geophysics, **40**, 224–232, doi: 10.1190/1.1440520.
Whitham, G. B., 1974, Linear and nonlinear waves: John Wiley and Sons.
Wyckoff, R. D., and H. G. Botset, 1936, The flow of gas-liquid mixtures through unconsolidated sands: Physics, **7**, 325–345, doi: 10.1063/1.1745402.
Zener, C., 1948, Elasticity and anelasticity of metals: University of Chicago Press.